AOARD REPORT
Contract No. 064043

FGM (Functionally Graded Material) Thermal Barrier Coatings for Hypersonic Structures – Design and Thermal Structural Analysis

Sook-Ying Ho, Andrei Kotousov, Phuc Nguyen, Steven Harding,
John Codrington and Hideaki Tsukamoto

Department of Mechanical Engineering
The University of Adelaide
Adelaide, SA 5000
AUSTRALIA

29 June 2007

AOARD Program Manager: Dr. J. P. Singh

Report Documentation Page

Form Approved
OMB No. 0704-0188

1. REPORT DATE	2. REPORT TYPE	3. DATES COVERED
14 NOV 2007	**Final**	**30-05-2006 to 21-08-2007**

4. TITLE AND SUBTITLE
FGM (Functionally Graded Material) Thermal Barrier Coatings for Hypersonic Structures ? Design and Thermal Structural Analysis

5a. CONTRACT NUMBER
FA48690610074

5b. GRANT NUMBER

5c. PROGRAM ELEMENT NUMBER

6. AUTHOR(S)
Sook Ying Ho

5d. PROJECT NUMBER

5e. TASK NUMBER

5f. WORK UNIT NUMBER

7. PERFORMING ORGANIZATION NAME(S) AND ADDRESS(ES)
University of Adelaide,Adelaide,Adelaide ,Australia,AU,SA 5005

8. PERFORMING ORGANIZATION REPORT NUMBER
N/A

9. SPONSORING/MONITORING AGENCY NAME(S) AND ADDRESS(ES)
AOARD, UNIT 45002, APO, AP, 96337-5002

10. SPONSOR/MONITOR'S ACRONYM(S)
AOARD-064043

11. SPONSOR/MONITOR'S REPORT NUMBER(S)

12. DISTRIBUTION/AVAILABILITY STATEMENT
Approved for public release; distribution unlimited

13. SUPPLEMENTARY NOTES

14. ABSTRACT
A feasibility study of a relatively simple and economical method for producing functionally graded thermal barrier coatings using the Wet Powder (Slurry) and Sintering method showed promising results. This method is relatively undeveloped and under utilised compared to more expensive techniques such as chemical vapour deposition, physical vapour deposition, plasma spraying and powder metallurgy. It utilizes a pressurized spray gun to spray a slurry mixture of the powdered coating material suspended in a liquid solution directly onto a substrate surface followed by sintering using an oxyacetylene torch. The effects of slurry composition, type of ceramic powder, compatibility with substrates, spraying and sintering conditions were studied. Several TBC specimens have been fabricated under various conditions to develop a procedure which produce good quality coatings (of up to 3 layers) with little or no spallation. The optimum time, heat flux and applied pressure level for sintering were deduced. TBCs produced from a 40-45% ceramic, 4% binder and 0.4% dispersant composition and sintered for 30 minutes with an applied pressure of 30 MPa produced good quality coatings with a uniform and very smooth surface. Scanning electron micrographs of the fabricated TBC coatings showed good contact between the grain boundaries of the ceramic powder. In phase 2 of this project, the Wet Powder and Sintering method will be further developed. Improvements to this method include automating the sintering procedure and optimizing the fabrication conditions. A much more extensive micromechanical testing program will be conducted to obtain a more qualitative measure of the quality of the FGM thermal barrier coatings and to develop high temperature constitutive models for input into the FE modeling. Additionally, the TBCs will be applied to realistic hypersonic structures such as a cylindrical combustor and tested under realistic combustion conditions.

15. SUBJECT TERMS					
16. SECURITY CLASSIFICATION OF:			17. LIMITATION OF ABSTRACT	18. NUMBER OF PAGES	19a. NAME OF RESPONSIBLE PERSON
a. REPORT **unclassified**	b. ABSTRACT **unclassified**	c. THIS PAGE **unclassified**	**Same as Report (SAR)**	**54**	

Standard Form 298 (Rev. 8-98)
Prescribed by ANSI Std Z39-18

Table of Contents

1. Introduction

In the past five years there is a renewed interest in hypersonic flight vehicles after the success of the Australian HyShot 2 fight test in 2002 and the two NASA X-43a flight tests in 2004. Hypersonic / high supersonic vehicles will experience increased heating, aerodynamic and aeroacoustic loads. Severe aerodynamic heating in hypersonic flight could cause structural deformation that can alter the flow properties around the vehicle, and therefore performance. Additionally, the potential for thermal and acoustic fatigue damage will be present and needs to be addressed to meet the mission life requirements of re-useable high speed vehicles. Consequently, there is an increasing requirement for high temperature materials, tools to predict the aerothermal loads, material behaviour and thermal-structural response.

Ceramic-metal functionally graded materials (FGMs) have been attracting a great deal of attention as thermal barrier coatings (TBCs) for aerospace structures working under super high temperatures and thermal gradients. FGM is a relatively new concept involving tailoring the internal microstructure of composite materials to specific applications, producing a microstructure with continuously varying thermal and mechanical properties at the continuum or bulk level. Hence, they are ideal for applications involving severe thermal gradients, such as the environments encountered by hypersonic flights because the microstructural grading of FGM TBCs could be adjusted to help reduce the mismatch in thermomechanical properties, which induce high thermal stresses in the structure.

This report is on Phase 1 of a three-years study to investigate the fabrication of advanced thermal barrier coating materials, such as ceramic-metal FGMs (which have high heat resistance and low thermal stress properties under high temperature conditions), the development of micromechanics models and aero-thermal-structural predictive tools, as part of a strategy to design advanced thermal barrier coatings for application to hypersonic vehicles.

The main focus of Phase 1 of this project is on the feasibility of using the Wet Powder (Slurry) Spray and Sintering method for the design of graded thermal barrier coatings for hypersonic structures. Theoretical and experimental studies on the design and optimisation, fabrication, and thermo-mechanical testing and modelling of FGM coated materials / structures will be conducted, with the view to achieve high

efficiency of the thermal coating by this method and ensure the required thermal protection of the structure under hypersonic flight conditions. The Wet Powder Spray method utilises a low-pressure spray to coat the surface with a mixture of ceramic powders, metal powders and binder (polymer). After application of the mixture to the surface, the coatings are heated to a sintering temperature during a specified period of time to achieve a suitable microstructure. Coating materials to be used in this method rely upon the physico-chemical properties of the parent surface and required thermo-mechanical properties of the thermal barrier. The selection of the composition and gradation of the coating materials represents the major challenge of the project.

Theoretical modelling of the thermo-mechanical and fracture behaviour of FGMs is critical to the design optimisation of graded thermal barrier coatings. Analytical methods of predicting the thermal stresses in the ceramic-metal FGM are formulated based on a combined micromechanics and fracture mechanics approach[1-6]. State-of-the-art techniques, developed in our previous studies[7, 8] to predict the aerothermal loads and structural response of high speed vehicles are presented, with the view to implement the FGM micromechanics models in the thermal-structural finite element (FE) codes. In Phase 2 of this study, the combined micromechanics / fracture mechanics model will be implemented in FE codes to predict the thermal-structural response of hypersonic structures (e.g. leading edges, engine) with FGM thermal barrier coatings.

WORK PLAN

An experimental program on the Wet Powder (Slurry) Spray and Sintering method and assessment of previously reported results in the literature from other TBC application methods are conducted to establish whether FGM thermal barrier coatings could be fabricated using technologically and economically viable processes. Experimental and theoretical studies are undertaken to characterise the thermal, mechanical and fracture properties of the FGMs and to assess their suitability for use as thermal barrier coatings for super high temperature applications.

The *experimental component* of Phase 1 of this project is a feasibility study on the application of the Wet Powder Spray and Sintering method to coat ceramic and composites onto metal substrates. Design optimisation and grading of the properties of thermal barrier coatings produced by this method, to achieve the desired thermal and mechanical properties, will be investigated in Phase2.

The *theoretical component* of Phase 1 of this study reviews state-of-the-art techniques available for predicting aerodynamic heating and structural response of high speed vehicles and issues associated with controlling the surface temperature of thermal barrier coated materials. Micromechanics modelling and analytical methods to predict thermal stresses in FGMs are discussed. In Phase 2, the micromechanics models developed in this study will be implemented in the FE thermal-structural models for parametric design studies of the global response of hypersonic structures coated with FGM thermal barrier coatings. In particular, the effect of the coating thickness and FGM properties will be investigated.

Milestones

- *Feasibility studies of the Wet Powder Spray and Sintering method (Phase 1)*

Compatibility analysis of ceramics and composites that can be used as graded layers will be conducted. Various candidates of ceramics and composites for the use in graded coating will be analysed for possible chemical and thermal reactions during manufacturing and operation at high temperatures. The surface integrity of the coatings will be investigated to assess the feasibility of using this simple and economical yet relatively undeveloped method to fabricate ceramic-metal FGM thermal barrier coatings.

- *Microstructure and thermo-mechanical testing (Phase 2)*

A simple test rig for manufacturing and testing of the graded thermal coating will be developed[9]. The rig will be designed to produce the desired graded coating layers on a base metal with subsequent testing of the integrity, microstructure and thermo-mechanical properties using standard facilities available at the School of mechanical Engineering and Adelaide Microscopy Centre at the University of Adelaide. Failure analysis will also be carried out with the view to adjusting the fabrication process and parameters to reduce interfacial spallation.

- *Micromechanics modelling of multi-phase composites (Phase 1 and 2)*

A micromechanical model of graded thermal coating based on our previous studies, by Kotousov and Tsukamoto[1-6], to describe the thermal and mechanical properties of the coating will be developed. In particular, the theories of transformation toughening

and constitutive equations of multi-phase composites will be developed. The micromechanical model will account for the effects of mismatch in material properties of coating layers and can describe the relationship between microstructure and macro characteristics of the multi-phase composite. The constitutive equations of multi-phase composites at elevated temperatures will be formulated to take into account stress concentration, thermal expansion, creep deformation of each phase, plastic deformation in the metal phase, and mass transfer at the interface between the ceramic and metal phases.

- *Finite element method modelling of thermal-structural response of FGM coated structure (Phase 1 and 2)*

The micromechanical model will be used in FE codes together with Computational Fluid Dynamics (for predicting the aerodynamic heat fluxes encountered in hypersonic flights) to model the global thermo-mechanical response of the structure. The effect of material properties, number of phases, phase degradation and microstructure will be investigated using FEM and the developed micromechanical models of constitutive behaviour from the above section. The thermo-mechanical response of the graded coatings will be compared to the results from the previous studies and to the observations from the experimental studies from the above sections. This study will provide critical information on the effect of particle size, composition, phase distribution and temperature on the thermo-mechanical properties and failure behaviour of FGMs to assist in future design optimisation studies.

2. Feasibility Studies of the Wet Powder (Slurry) and Sintering Method for Fabricating FGM Thermal Barrier Coatings

The most common ceramic material used in Thermal Barrier Coatings is zirconia (ZrO_2). Zirconia is found in a monoclinic phase structure within a temperature range 22 to 1170ºC, with high hardness, toughness and very low thermal conductivity and is regarded as having good sinterability for use in forming solid volumes from a packed powder[10]. It maintains a monoclinic phase structure for temperatures up to 1170ºC at which point it changes to a tetragonal phase structure with decreased density. Consequently, a problem in using pure zirconia in TBC's is that during cooling the phase change from a tetragonal to monoclinic structure causes a 3 to 5 percent increase in volume of the zirconia ceramic. As a result severe cracking propagates throughout the ceramic, rendering it useless as a TBC. To overcome this effect a stabilising oxide capable of being dissolved in the zirconia ceramic structure is added to form a permanent cubic phase within the microstructure. The permanent cubic phase regions slow down the phase change process to prevent cracking within the structure during cooling[11]. Common oxide additives include Magnesium Oxide (MgO), Calcium Oxide or lime (CaO) and yttria (Y_2O_3). Depending upon the mol % of oxide added, the zirconia is classified as either partially stabilised or fully stabilised. Partially stabilised zirconia still maintains a monoclinic phase at low temperatures however fully stabilised zirconia remains in a cubic phase at temperatures below its melting point.

In the past decade, many techniques have been described in the literature for fabricating and manufacturing Functionally Graded Materials. There are two main means, mechanical and chemical processes, of applying the material coating to the metal substrate. However, of the two application processes, the mechanical means offer the most robust methods for producing surface coatings in terms of economics, adaptability to large and complex surfaces, different coating and substrate materials and fabrication difficulty. In particular the Electron Beam Physical Vapour Deposition, Powder Flame Spraying, Plasma Thermal Spray and Cold Gas Dynamic Spray Coating techniques are particularly suited for creating thermal barrier coatings. These techniques however, are expensive and impractical for small-scale production. This study will focus on the relatively under developed Wet Powder Spray and Sintering method for producing thermal barrier

coatings[9]. This method is not as highly utilised as the other techniques and it is desirable to determine whether it can produce TBC coatings of comparable quality.

Wet Powder Spraying

The wet powder spraying (WPS) method for producing powder coatings largely involves suspending the powdered coating material in a liquid solution to create a slurry mixture which is then sprayed directly onto a substrate surface using a pressurised spray gun. The WPS process can create coatings on surfaces with almost any geometry with surface thicknesses between 5 to 100 micrometers[12]. The consistency of the sprayed coating is controlled by spraying conditions such as the spray pressure, spray distance and nozzle type and also through the viscosity and level of solid suspension within the slurry.

To create the slurry mixtures the coating material is mixed with an appropriate solvent, typically distilled water, until the desired viscosity is obtained. To assist the dissolution of the coating powder within the solvent, a dispersant is used to prevent the separation of the coating material from the solvent. The slurry solution is sprayed directly to a substrate surface and allowed to dry. Typically thin coating thicknesses are produced to prevent surface cracking due to shrinkage during the drying stage[12]. Thicker coatings are created by building successive dried layers upon the substrate surface.

Sintering

The sintering process essentially involves using a high temperature thermal flux to heat up powder particles to a point where they bond together to form a uniform body. During sintering the loosely arranged powder particles coalesce to shrink the total material volume, which results in reduced porosity and increased density of the sintered volume, to produce a more integral material structure while still maintaining the initial material properties of the powder.

Initially the powder particles are in loose contact with one another, without any inter particle bonding. With the initial addition of thermal energy, the grain boundaries grow in the contact areas between powder particles to form necks between them. As more thermal energy is supplied the grain boundaries continue to grow and envelope a single void to create a spherical pore within the final microstructure. The principal effect that drives the sintering process is the reduction

surface area of the powder particles where the surface energy of a particle is of a greater magnitude than that of the particles grain boundary energies. Therefore the total energy of the powder particles is reduced by a decrease in surface area and increase in grain boundary. The sintering process is particularly suited to metals and ceramics with very high melting temperatures. This makes sintering an ideal manufacture method for thermal barrier coatings which are typically manufactured using high temperature ceramics that are initially produced in a powdered form.

Sintering can be conducted on a specimen using a variety of methods. Traditionally sintering is conducted using high temperature ovens or kilns, which have an advantage over other sintering methods as the specimen can be sintered in a controlled thermal environment at a wide range of temperatures for any time duration required. Another method involves using high intensity lasers to sinter thin material volumes. The sintering takes place for very short durations with large temperatures in a localised region on the surface of the specimen. Lastly sintering can also be conducted on a specimen using a direct combustion stream, such as with an oxyacetylene or propane torch[13]. Direct combustion stream temperatures can reach up to 3000ºC however, while being the simplest sintering method, creating a uniform heat flux on the specimen is difficult and the sintering temperature range is limited. The present study will utilise this simple oxyacetylene torch method for sintering. To achieve a more uniform coating, an automated sintering platform[9] has been designed to enable automation of the sintering process. Phase 2 of this project will undergo a more detailed investigation of the automated sintering method of producing high quality FGM coatings.

2.1 Material Selection and Compatibility Studies

2.1.1 Coating Composition

Ceramic

The most important component of a Thermal Barrier Coating (TBC) material is the ceramic used to supply the bulk material properties for the coating. The ceramic must first satisfy the primary design requirements of low thermal conductivity and temperature resilient microstructure, however some secondary characteristics such a solubility and corrosion resistance must be considered in the ceramic selection process.

The wet spray process requires the coating to be prepared in a slurry phase, which is a mixture of solid particles suspended in a liquid. In order to be suspended within a liquid the ceramic particles must be small enough to allow for dispersive forces to overcome gravitational forces to prevent the ceramic simply forming sediment within the slurry solution. The magnitude of the dispersion and gravitational forces are dependant on the ceramic particle geometry and density, smaller particles tend to attract larger dispersion forces and denser particles are more susceptible to gravitational forces. To prevent separation of the ceramic and solvent during and after mixing a dispersant is added to the TBC slurry mixture. Sedimentation of the ceramic causes disruption to the wet spray process by potentially blocking the spray nozzle or forming an uneven distribution of the ceramic over the substrate surface.

During the wet spray process the ceramic is initially immersed in a mildly acidic solution and later sprayed in an open atmosphere and exposed to high temperature. In an acidic environment ceramics can undergo leaching, a process where ceramic phases along the grain boundary react with hydrogen ions to form a soluble material that is washed away by the solvent. Alternatively during sintering, the high temperature environment can induce volatilization whereby a ceramic phase can be stripped of oxygen to form a separate phase with reduced oxygen content.

After considering the material requirements for the TBC ceramic yttria stabilised zirconia (YSZ) was selected. For the purposes of this experimental investigation, YSZ satisfies all the material requirements necessary for the wet spray and sintering process. Also, there is a large volume of reference material on traditionally manufactured YSZ coatings for comparison with our experimental TBC produced using the wet powder spray method. The ability to determine how these TBC's compare to traditionally manufactured YSZ coatings is invaluable in forming an objective appraisal of the usefulness of the wet powder spray technique.

Dispersant

To ensure a uniform suspension of the ceramic within the slurry a dispersant is required to assist ceramic absorption within the solvent and prevent separation. Slurries with low ceramic to solvent ratios do not typically require dispersants as the solvent still maintains a high rating of absorption potential. However as the ceramic to solvent ratio increases, the viscosity of the slurry mixture also increases to a point

where additional ceramic powder becomes insoluble in the slurry mixture. The molecular form of the dispersant is comprised of two distinct sections, one section molecularly similar to a ceramic and another similar to a solvent molecule. Both ends of the dispersant molecule form secondary bonds with the ceramic and solvent molecules allowing the ceramic to be absorbed by the surrounding solvent. The dispersant essentially increases the viscosity of the slurry, making it easier to spray for larger ratios of ceramic to solvent.

The dispersant chosen for creation of the Thermal Barrier Coating is Tetra Sodium Pyrophosphate.

Binder

The Binder forms an integral function in the formation of sintered thermal barrier coatings by maintaining contact between powder particles after drying and maintain the structural integrity of the coating prior to sintering . A binder acts as a cementing medium between the powder particles by filling void areas between particles to prevent movement. In essence the binder and ceramic powder particles form a composite with the ceramic powder acting as a reinforcement phase and the binder as a matrix phase. The binder is designed to vaporise at low temperatures compared to the sintering temperature of the ceramic powder and be soluble in the slurry solvent. Before sintering the binder is vaporised from the coating in a process called debinding. Debinding requires the ceramic powder to have a moderate level of porosity to allow the vaporised binder to be fully removed from the coating. Neglecting the debinding stage prior to sintering could introduce contaminants within the sintered ceramic microstructure due to reactions between the binder and the ceramic grain boundaries.

Based upon the promising results reported by Roy et. Al[14] in creating sintered YSZ beads, a copolymer of styrene and acrylic ester or hydrosoluble polyvinyl alcohol were considered as suitable binders for the wet powder spray slurry. Ultimately hydrosoluble polyvinyl alcohol was selected as it was comparatively inexpensive and easily sourced from local chemical suppliers.

Substrate

To determine the effectiveness of the Thermal Barrier Coatings (TBC's) to industrial applications, substrates representing typical industrial

metal surfaces were used as platforms for the spraying and sintering of TBC's using the Wet Powder Spray method. The three substrate materials selected for this investigation are Mild Steel, Stainless Steel and Inconel. Some average substrate thermal properties applicable to the use of TBC's are shown in Table 1.

Table1: Substrate Thermal Properties[15]

Substrate Material	Melting Point (ºC)	Coefficient of Thermal Expansion (μm/mK)	Conductivity (W/mK)
Mild Steel	1515	11.7	51.9
Stainless Steel	1528	10.8	16.2
Inconel	1410	12.8	9.8

Ideally the substrate surface will have a similar coefficient of thermal expansion as the TBC to prevent thermal stresses developing during temperature changes. As ceramics typically have very low coefficients of thermal expansion it is expected that coatings produced on stainless steels will be the most resilient to fatigue due to induced repetitive thermal stresses.

The substrate surfaces are initially prepped for spraying by sanding the surface with an orbital sander using a medium grit metal sanding pad. The sanding process typically leaves a fairly polished surface without any signs of surface oxidation. Following the sanding process the surface is wiped with methylated spirits to clean any residue or metal oxide. It is essential the substrate surface is clear of any loose particles to promote a secure bond between the coating and substrate and to reduce the effect of contaminates within the TBC microstructure.

2.2 Manufacture Process

2.2.1 Mixing procedure

Initial slurry compositions are created using a mixing procedure utilised in creating sintered beads of Yttria Partially Stabilised Zirconia (YSZ)[14]. Initially a volume of distilled water solvent is agitated using a magnetic mixing element in a beaker placed on a magnetic mixing pad. Heating of the mixture is not required. Tetra

Sodium Pyrophosphate dispersant is slowly added to the agitated solvent and allowed to mix. The ceramic powder is then added to the mixtures at a slow even rate to form a more viscous mixture. After ensuring the ceramic has been fully absorbed by the solvent the pH of the slurry is adjusted to create a slightly acidic solution. To adjust the slurry pH, small amounts of dilute solutions of hydrochloric acid HCl and sodium hydroxide NaOH are used. Finally hydrosoluble polyvinyl alcohol binder crystals are slowly added to the slurry mixture. The addition of the binder greatly increases the viscosity of the slurry, requiring the binder to be added to the mixture at a gradual rate with an increased rate of mixture agitation. The binder has a tendency to form solid lumps within the slurry if introduced into the mixture at too fast a rate. Typically the slurry mixture variation is centred upon a base mix of 40-50 wt% yttria partially stabilised zirconia, 45 wt% polyvinyl alcohol, 0.4 wt% Tetra Sodium Pyrophosphate and the remaining portion is the distilled water solvent.

2.2.2. Spraying

Spraying the Thermal Barrier Coating (YBC) slurry mixture onto the substrate resembles similar spray processes used to coat surfaces with powder based paints. To spray the TBC slurry a regular gravity fed paint spray gun is connected to a small air compressor and used to spray the slurry mixture fed into the spray gun from a top mounted paint hopper. The spray gun operates by feeding the high velocity compressed air through a reduced pipe section where, according to the Venturi Affect the fluid velocity rises and pressure falls. At this point the reduced pressure gradient draws in slurry from a tube fed into the air stream and the high fluid velocity atomises the slurry into discrete particles within the air stream. The stream is then directed at the TBC surface to deposit the slurry particles in a uniform layer.

Important material factors affecting the ease in which the slurry is sprayed are the viscosity and level of suspended solids within the slurry mixture. As the viscosity of the slurry increases, the ability of the spray gun to draw slurry into the air stream and atomise it is reduced due to the increased viscous shear forces. To overcome the higher viscous forces the stream pressure and thus flow velocity are increased at the cost of a reduction in the final coating thickness. To prevent clogging of the slurry injector and spray nozzle, any suspended solids need to be prevented from forming within the slurry mixture prior to spraying using a dispersant during the mixing process.

The spraying technique used to spray the TBC onto the substrate involves using several quick passes of the spray jet over the substrate surface to form an even coating. The spray nozzle is kept around 25cm from the surface to allow a large cone shaped spray stream and prevent rapid deposition of the slurry on the surface. The pressure of the spray stream is varied from 20 to 80 psi, depending on the desired coating thickness. Thinner coatings are produced using the higher pressure ranges to fan out the slurry on the substrate surface and produce a fairly uniform and even finish. Lower pressures tend to spray larger slurry molecules onto the surface to give a more textured finish.

Using the wet powder spray method, the thickness of the TBC can be controlled from around 5 μm to 2 mm by varying the spray pressure and the number of spray passes over the coating surface. During drying, coatings with large thicknesses shrink to form uneven surface distributions. Initial tests carried out with 1mm thick coatings have led to cracking of the coating surface during the cooling of the coating after sintering. It is suspected that this is due to induced thermal stresses within the layer itself caused by large temperature gradient over the surface due to the high thermal conductivity of the coating itself. Also the mismatch in thermal coefficients of the substrate and coating is also suspected to induce thermal stresses within the coating and lead to spalling. This observed effect leads to the conclusion that the BC thickness is an important parameter in regards to the structural integrity of the final coating. Smaller layer thicknesses are expected to provide a more stable TBC.

2.2.3 Debinding and Sintering

To investigate the effects of different debinding and sintering methods the sprayed and dried Thermal Barrier Coating (TBC) specimens are subjected to a combination of debinding and sintering. The three scenarios for the debinding and sintering process involve using an oven to firstly debind the coating and then immediately continue to sinter the coating, debind the coating within the oven and then remove to be sintered using an oxyacetylene torch or use an oxy acetylene torch to simultaneously debind and sinter the coating.

To debind and sinter the TBC specimens using the oven the oven is first preheated to 300ºC while the TBC specimen dries after spraying. Once dry the TBC is placed in the heated oven for debinding for 30 minutes. Over this time period the

hydrosoluble polyvinyl alcohol begins to be vaporised at 230 ºC to form carbon dioxide and water vapour which do not react with the ceramic powder coating. After debinding the oven temperature is increased to 800 ºC to sinter the powder coating over two hours. After this time period the specimen is removed form the oven and allowed to cool in the open atmosphere. Initial tests found the TBC specimens debinded and sintered using this approach did not form rigid surface layers. When subjected to light surface agitation the coating would break away from the substrate either as large flakes or as a fine powder.

Coatings debinded in the oven and then sintered with an oxyacetylene torch undergo the same debinding procedure where dried specimens are placed in a preheated 300 ºC oven for 30 minutes to debind. The specimens are then removed from the oven and allowed to cool before being sintered with an oxy acetylene torch. The specimens sintered using the oxy acetylene torch are subjected to different heat fluxes controlled by holding the combustion flame at variable distances from the TBC surface for variable lengths of time.

The final debinding and sintering method is the simplest where dry specimens are simultaneously debinded and sintered with an oxy acetylene torch. As stated previously the heat flux to the surface is controlled by varying the flame distance from the TBC surface and the time spent heating.

2.2.4 Testing

Two important parameters that are to be tested are the conductivity of the TBC surface and the structural durability of the TBC layer. The following tests were used for preliminary testing of the TBCs manufactured by the different debinding and sintering methods described above.

Conductivity

To measure the conductivity of the TBC in a direction normal to the surface an axial flow method will be adopted. The simplest axial flow method is the comparative cut bar technique where the conductivity of the TBC and the substrate is determined as a whole. The specimen is sampled between two plates made of a reference material with a known thermal conductivity. Hence, the overall conductivity of the specimen can be calculated using the cross sectional lengths of the two reference samples and the specimen, the thermal gradients over the two reference

samples and the specimen and also the thermal conductivity of the reference material[9].

Structural

Standard structural testing techniques will be applied to discern the durability of the coating. However, for preliminary assessment of the quality of the TBCs, a simple test to assess the toughness of the TBC's is through simple surface scratching. The top surface of the coating is scratched using a steel edge to discern if the layer has any toughness and durability that could be meaningfully measured.

3. RESULTS - Microstructure and Preliminary Thermo-mechanical Testing

As very little details are available in the open literature on the processing and fabrication procedures for the Wet Powder and Sintering method, the initial experiments were by trial and error to produce a working TBC sample. The lessons learnt and some useful observations are noted in this section of the report.

Certain ceramic powders are more suited for the Wet Spray and Sintering Method than others. It was found that TZ-3Y-E, which is a partially stabilised zirconia powder, was particularly suitable. The percentage of ceramic powder which was found to work well was 45%, while 50% produced many large particles and slightly lumpy slurry. The optimum amount of binder was found to be 4%. A higher amount would produce a slurry that is too vicious to spray.

Preparation of the specimen surface was quite important to the adherence of the coating to the substrate. The surface of the substrate was sanded down to a certain roughness, and the excess residue was removed using methylated spirits. The optimum number of coating layers was found to be four layers and the most suitable applied pressure to the surface was 30MPa. The application of the surface pressure greatly reduced the sintering time. To ensure surface integrity, it is recommended that each layer should be left to dry for 2 hours between application of coats, and at least 3 hours after the final coat.

The sintering time that achieved a good coating was found to be 30 minutes. The distance of the oxy-acetylene torch from the substrate should be such that the flame is just reaching the surface, so that only a small heat flux is applied to the surface. The cooling environment was also found to be critical - the coatings had a tendency to crack during the period after sintering if the weather conditions are too cold. It was found that after sintering, leaving the specimens in the oven at 300ºC produced a good coating.

Different percentages of ceramic powder and binder

Testing consisted of seven distinct slurry compositions. Samples were created using different debinding and sintering techniques for each composition, as shown in Table 3-1.

Table3-1: Slurry Compositions

Composition	Ceramic %	Binder %	Dispersant %
1	40	4	0.4
2	45	4	0.4
3	50	4	0.4
4	40	5	0.4
5	45	5	0.4
6	40	6	0.4
7	45	6	0.4

The following observations were made from the production of TBC's using different variations of substrate, surface preparation, composition as listed in the above Table, coating thicknesses and sintering durations. The greater the thickness of the coating, the more prone it is to cracking. This was evident on the edges of the specimen, which tended to form large flakes upon oxyacetylene sintering as shown in Figure 3-1, or a fine disassociated powder after oven sintering.

Figure 3-1: Surface Flaking During Oxy Acetylene Sintering

The wet powder coatings created from composition 2 and 3 slurry mixtures produced a more uniform thickness after spraying and remained more adhesive to the substrate surface than the other five compositions tested. Compositions 4-7 proved to be quite unsuccessful, with small increases in the percentage of binder yielding much more viscous slurry. This caused difficulties in spraying the ceramic slurry, and it produced a very uneven and lumpy surface coating

When sintering is undertaken with the oxyacetylene torch the surface undergoes a transition from a white powder coating to a solid brown textured layer as shown in Figure 3-2. However, after continued sintering this solid coating transforms into a white powdery coating without any adherence to the substrate.

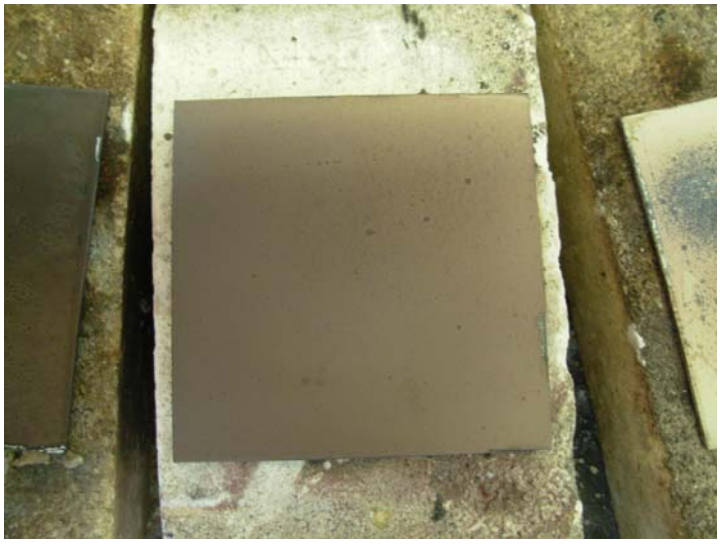

Figure 3-2: Durable Lightly Sintered Thermal Barrier Coating

The sanded substrate surfaces tend to offer a slightly more adhesive surface, due to the surface roughness giving something for the slurry to adhere to. The remaining residue from sanding is removed with methylated spirits.

With these experiments it was found that the coatings of thickness greater than 1mm tended to crack easily. In order to achieve thicker coatings, the next stage of this experimental program experimented with multi-layered coatings, as well as different ceramic power combinations.

Different ceramic powder combinations and multi-layered coatings

The current ceramic powder that was being used was a fully stabilised zirconia powder TZ-0Y. However a readily available powder TZ-3Y-E, partially stabilised zirconia powder, was available and utilised. These tests consisted of a combination of 3, 4 and 5 layers. In the previous tests, the thickness of each coat was relatively small, hence to produce a more viable thermal coating, multiple coats needed to be applied. In fabricating the multilayered coatings, the sintering times were varied from 10 to 20 minutes.

From these tests, it was discovered that the optimal number of layers was 3-4 layers. Samples with five or more layers usually lead to rapid failure during sintering. After experimentation, the sintered specimens were still of a low quality, however the difference in quality between the 2 powders was quite visible. The ceramic powder TZ-0Y tended to flake and spall significantly more than TZ-3Y-E under the same thermal loading conditions. This can be seen in Figure 3-3. It can be concluded that partially stabilised zirconia powder worked best for our methodology.

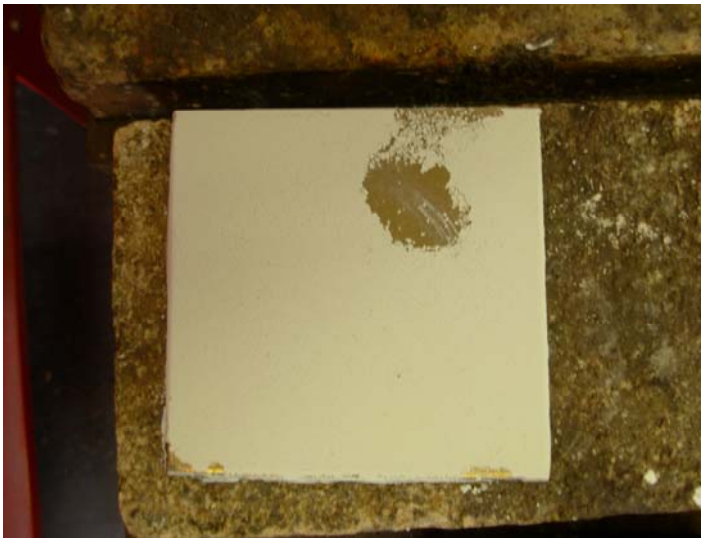

Figure 3-3: Sintered Surfaces a) Ceramic Powder TZ-0Y

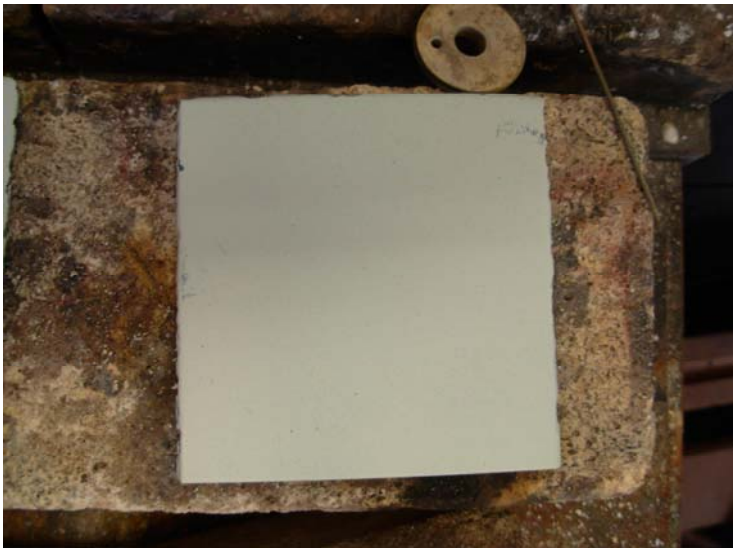

Figure 3-3: Sintered Surfaces b) Ceramic Powder TZ-3Y-E

The overall quality of the coating was improving, but it still had poor surface toughness, and could be easily damaged. It was concluded that the coating was still not properly sintered, as the sintering times were too short. However if the specimen was sintered for an hour, there would be no chalky residue. Sintering times longer than an hour was considered to be too excessive for a small area. A literature search found that sintering times could be decreased with applied pressure. The next set of tests investigates the effectiveness of applied pressure on the sintering time.

Effect of applied pressure on sintering times

In the previous tests it was found that the surface area of the substrate was too large for the heat to be distributed evenly from the oxyacetylene torch. The centre of the substrate of the applied coating was experiencing the sintering effect, while the edges of the substrate were not (the edges still had a chalky residue). Thus in the next set of tests, the substrate size was reduced from 100mm x 100mm to 50mm x 50mm.

Another aim was to reduce the time of sintering. From the literature it was found that applying pressure reduces the sintering time. After the coatings were applied to the substrate and before the sintering process, pressure was applied to the surface. The amount of pressure applied to the specimens was varied ranging from 10,

20, 30, 40, 50, 60 MPa. The sintering times were also varied ranging from 15, 20, 25 and 30 minutes.

The higher pressures produced an extremely smooth finish before sintering, making the coating denser. It was found that pressures greater than 40 MPa caused spallation at the edges after sintering, as shown in Figure 3-4. On the other hand, the specimens with an applied pressure of 30 MPa and below tended not to spall at the edges and produced an adequate coating. The applied pressure seemed to reduce the sintering time by half, as well as providing an extremely smooth and clean surface, which can be seen in Figure 3-5.

Figure 3-4: Failed specimen with applied pressure of 40 MPa

Figure 3-5: Successful specimen with applied pressure of 30 MPa.

While the sintering times had decreased by 50%, it was desirable to reduce the times further. For the next set of tests, experiments were performed on the effect of varying the heat fluxes, as well as a heating step.

Figures 3-6 (a) to (d) show the sintering taking effect over time. In each image, it can be seen that the grain boundaries increase in contact area with sintering time, eventually reaching the final sintering stage.

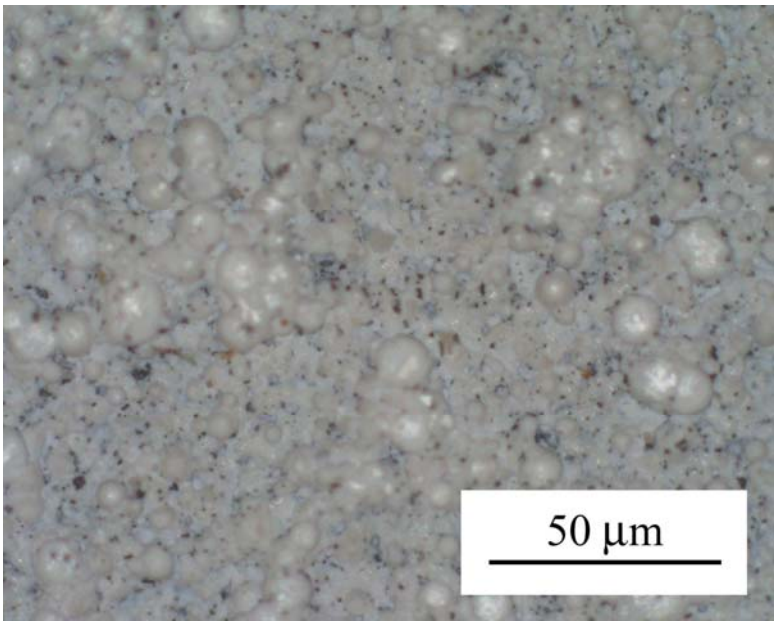

Figure 3-6: Sintering Stages a) 15 minutes

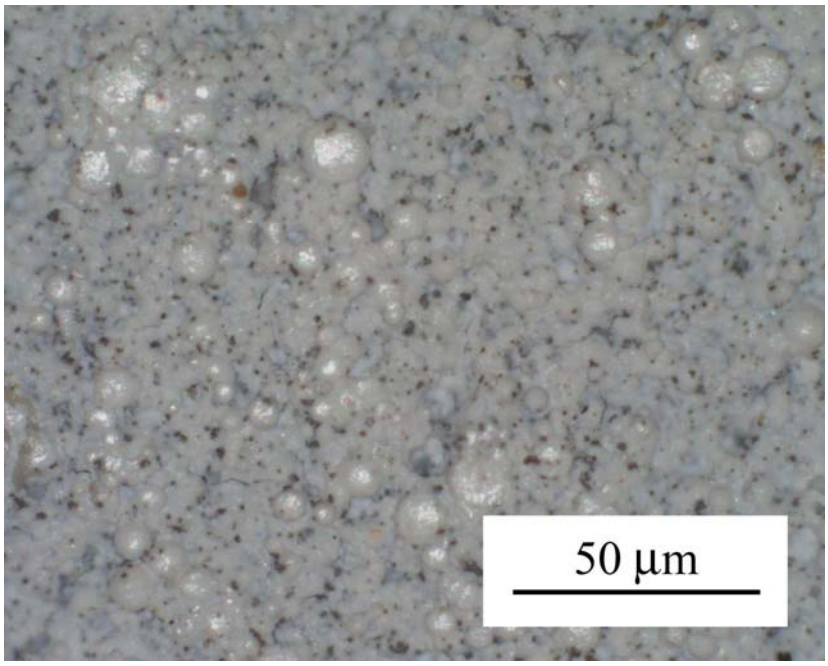

Figure 3-6: Sintering Stages b) 20 minutes

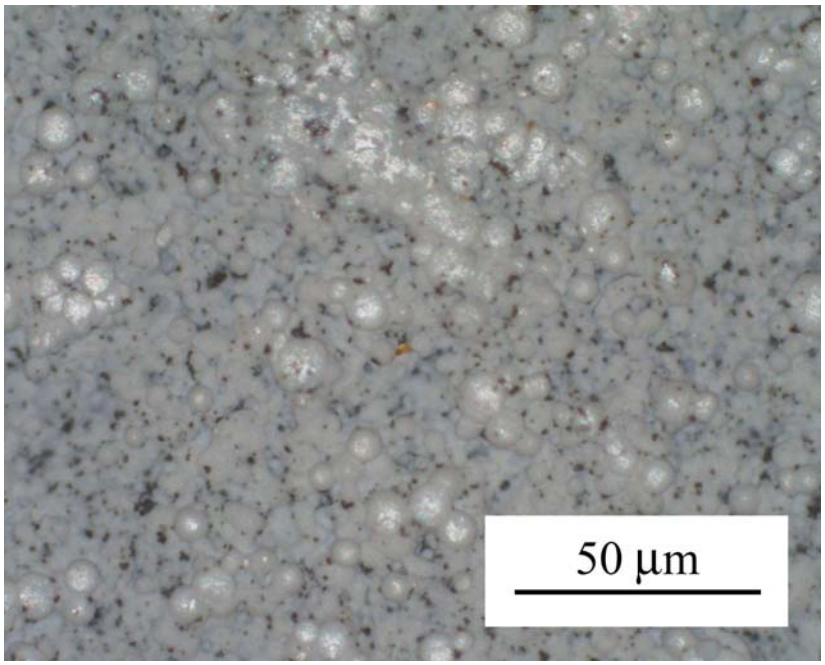

Figure 3-6: Sintering Stages c) 25 minutes

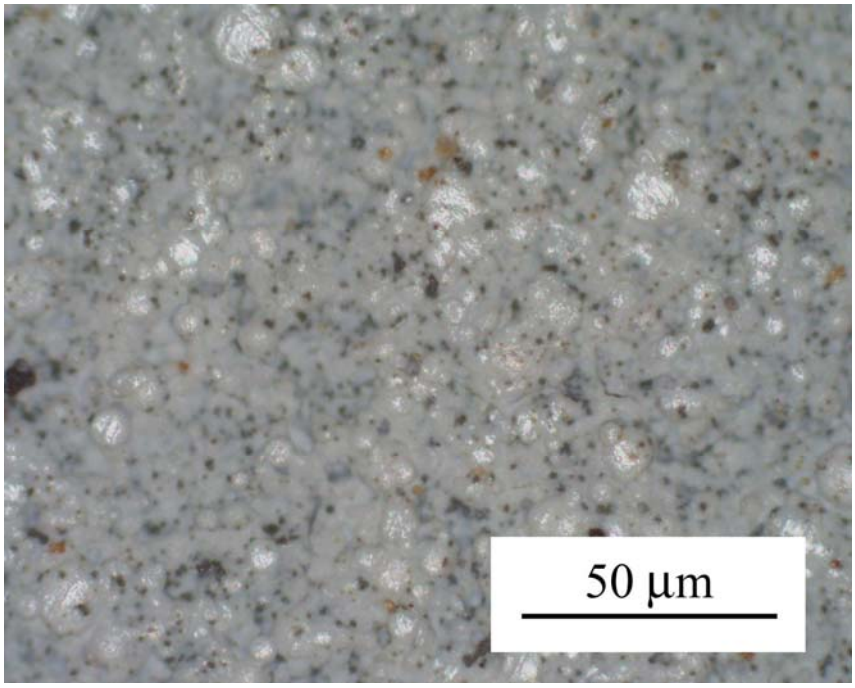

Figure 3-6: Sintering Stages d) 30 minutes

Effect of varying heat fluxes and heating step

This set of experiments attempt to reduce the sintering time by varying the heat fluxes. Earlier testing showed that small amounts of heat applied yielded the best results, whereas higher heat fluxes during sintering induced high thermal stresses too quickly, and consequently the rapid cooling causes the coating to spall and flake. The effect of applying small, medium or high heat fluxes to the specimens was studied. Experiments with a heat stepping was also investigated. This involved varying the heat flux from small to medium to high in steps on the individual specimen.

It was found that spallation did not occur when a small heat flux was applied, as observed in previous tests. When a medium heat flux was applied, the coating failed after sintering for 30 minutes. The coating where a high heat flux was applied to, failed 15-20 minutes into sintering. These results were as expected and confirmed our previous results. A heating step was then applied, where the specimen was heated for 30 minutes, with varying heat fluxes, as shown in Table 3-2.

Table 3-2: Heating Step Process

Heat Flux	**Time Sintered (minutes)**	**Progressed Time (minutes)**
Low	5	0 – 5
Medium	5	5 – 10
High	10	10 – 20
Medium	5	20 – 25
Low	5	25 – 30

The experiments with the added heating step produced coatings that looked very promising. The next phase will investigate coatings produced using the heating step procedure followed by leaving the specimens in an oven preset at 300ºC. Future studies will include a bonding layer between the substrate and the ceramic and/or a polymer coating on top of the TBC layers to prevent oxidation and surface damage.

3. Micromechanics Modelling of Multi-phase Composites

In order to maximise the benefits derived from FGMs, appropriate computational strategies that couple the heterogeneous microstructural properties of the TBC material with the global analysis of the response of the structure to the thermal environment need to be developed. This section of the report describes the development of micromechanics models for FGMs, based on the approaches used in earlier studies by one of the authors (Tsukamoto et. al[1-3]), that could be incorporated in the global FE analysis presented in the next section (Section 5).

So far a number of analytical and computational methods to predict thermal stress states in FGMs and design optimal FGMs have been proposed. Some of them considered macroscopic heterogeneity, and used the simple rules of mixture such as Voghit and Reuss rules to derive effective properties of the composites. Some studies take into more account the microscopic heterogeneity. These studies are classified into two categories. One adopts finite element methods, which assume periodic microstructure of compositions in FGMs[16-19]. The other is an analysis based on micromechanics, one of which is the Eshelby's equivalent inclusion method[21-23] being effective and applicable to analyze high-temperature behavior of ceramic-metal composites. An earlier work by Wakashima and Tsukamoto[1-2] applied the mean-field micromechanical concepts to estimating the thermal stresses in a FGM plate. To date, many studies have been done based on such micromechanical concepts[4-5].

From the viewpoints of what kinds of inelastic deformations for each phase to be taken into account, some studies[23] considered plastic deformation of metal phase, which is the time-independent deformation, and some studies[24] took into consideration time-dependent deformation such as creep in FGM plates, for which the constitutive relations derived from experimental results were used. Recently, micromechanical approach considering plastic deformation of metal phase and creep of metal and ceramic phase as well as diffusional mass flow at the interface between metal and ceramic phases is proposed by one of the authors[25].

An analytical and design method of ceramic-metal FGM TBCs based on the mean-field micromechanical approach considering time-dependent inelastic deformation such as creep and interface diffusion was presented by the authors at the Structural Integrity and Failure Symposium in September 2006[3]. In this study, Ni-ZrO_2 FGM thermal barrier structures are analysed numerically. The effects of the

compositional gradation patterns on the thermal stress states, especially maximum tensile micro-stresses in ceramic phases, are examined. The influence of time-dependent inelastic deformation on the stress states in FGMs is also investigated and the useful suggestions to design suitable FGMs have been made. The findings from this study[3] are described below.

4.1 OUTLINE OF ANALYSIS

4.1.1 FGM plates and thermo-mechanical loadings

The outline of the analytical method mentioned here is based on the study by one of the authors (Tsukamoto[25]). The illustration of a model of a TBC with an FGM structure is shown in Figure 4-1.

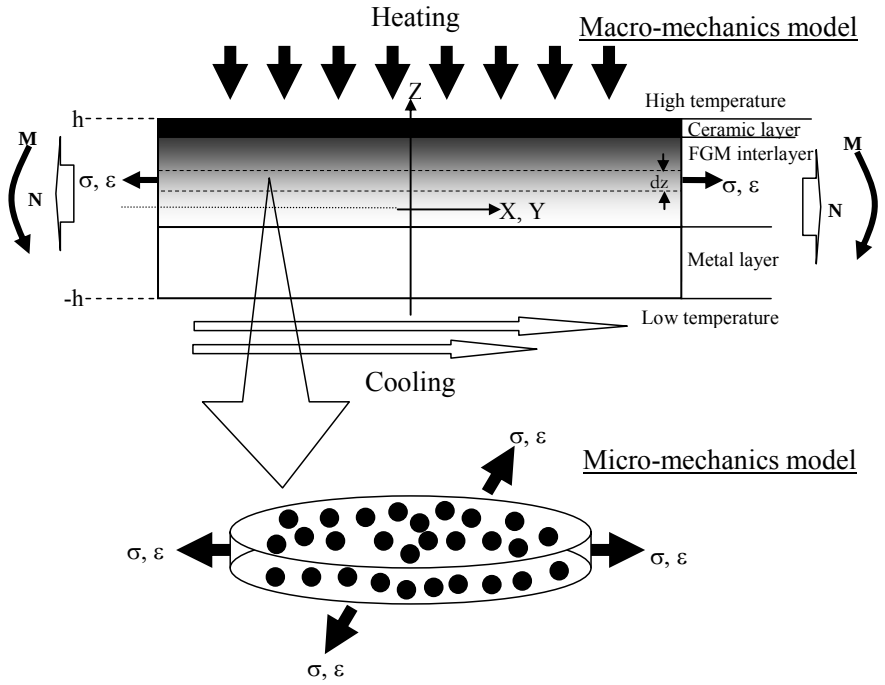

Figure 4-1.
Schematic illustration for macro- and micromechanical model for a thermal barrier coating with an FGM interlayer subjected to balanced bi-axial loadings.

The FGM TBC considered here has characteristics of a graded composition with spherical particles dispersing in the matrix. The unidirectional heat flow is assumed to be in the thickness direction. The temperature distribution $\theta(z,t)$ can be determined by solving the following equation.

$$c(z)\rho(z)\frac{\partial\theta(z,t)}{\partial t}=\frac{\partial}{\partial z}\left(\lambda(z)\frac{\partial\theta(z,t)}{\partial z}\right) \qquad (1)$$

where, $c(z)$ is the specific heat, $\rho(z)$ the mass density and $\lambda(z)$ the thermal conductivity. The effective thermal properties of composites can be derived from the mean-field micromechanics[16-17]. Mechanical loadings acting on the FGM plate are assumed equally biaxial in-plane force and bending moment. In the following, the analytical method to describe the thermal stresses in the FGM plate will be formulated from both micromechanical and macromechanical viewpoints.

4.1.2 Micromechanical approach

Macroscopically homogeneous composites with spherical particles are considered for the building block of the FGM plate as shown in Figure 4-1. The building-block composites are assumed to be subjected to a balanced bi-axial loading. In the following, the metal phase is assumed to be matrix and ceramic one is particles, which are indicated by subscript 0 and 1, respectively. The inversion of the relation of matrix and particles can be easily handled in the similar way. The constituents of the composites can be allowed to deform inelastically in this analysis, which means that it is considered that creep strain ε^c can be introduced in metal and ceramic phases, and plastic strain ε^p by yielding can be introduced in metal phase. In addition, the diffusional mass transport along the interface between metal and ceramic phases is also taken into account with a strain of ε^d. Such a micromechanical concept was introduced by Mori et al[26]. Because of the in-plane isotropy and constancy-of-volume law in the composites with spherical particles under balanced bi-axial loadings, the components of these inelastic in-plane micro-strains are assumed to be expressed as ε^p, ε^c and ε^d, while out-of-plane components are expressed as $-2\varepsilon^p$, $-2\varepsilon^c$ and $-2\varepsilon^d$, respectively. Then, in-plane and out-of-plane micro-stresses in each phase are shown as follows[25],

$$\begin{aligned}\sigma_0^{in} &= 2(\beta_0+1/3\gamma_0)\sigma+3f_1\beta^*(\alpha_1-\alpha_0)\theta \\ &\quad +2f_1\gamma^*\left\{(\varepsilon_1^c-\varepsilon_0^c)+\varepsilon^d-\varepsilon^p\right\}\end{aligned} \qquad (2)$$

$$\begin{aligned}\sigma_0^{out} &= 2(\beta_0-2/3\gamma_0)\sigma+3f_1\beta^*(\alpha_1-\alpha_0)\theta \\ &\quad -4f_1\gamma^*\left\{(\varepsilon_1^c-\varepsilon_0^c)+\varepsilon^d-\varepsilon^p\right\}\end{aligned} \qquad (3)$$

for the metal matrix (indicated by subscript 0) and

$$\sigma_1^{in} = 2(\beta_1 + 1/3\gamma_1)\sigma - 3f_0\beta^*(\alpha_1 - \alpha_0)\theta - 2f_0\gamma^*\left\{(\varepsilon_1^c - \varepsilon_0^c) + \varepsilon^d - \varepsilon^p\right\} \quad (4)$$

$$\sigma_1^{out} = 2(\beta_1 - 2/3\gamma_1)\sigma - 3f_0\beta^*(\alpha_1 - \alpha_0)\theta + 4f_0\gamma^*\left\{(\varepsilon_1^c - \varepsilon_0^c) + \varepsilon^d - \varepsilon^p\right\} \quad (5)$$

for the ceramic particle (indicated by subscript 1).

Here, f_0 and f_1 are volume fraction of metal matrix and ceramic particles, respectively, and σ is a macro-stress due to balanced bi-axial loadings. $\beta_0, \beta_1, \gamma_0, \gamma_1, \beta^*$ and γ^* are constants depending on the elastic constants and volume fraction of each phase, which are shown in detail in the study by Tsukamoto[25]. For these in-plane and out-of-plane micro-stresses, the following relations are satisfied.

$$f_0\sigma_0^{in} + f_1\sigma_1^{in} = \sigma \quad (6)$$

$$f_0\sigma_0^{out} + f_1\sigma_1^{out} = 0 \quad (7)$$

Further, the von Mises-type equivalent micro-stress in each phase are expressed as follows

$$\sigma_0^{eq} \equiv \left|\sigma_0^{in} - \sigma_0^{out}\right| = 2\left|\gamma_0\sigma + 3f_1\gamma^*\left\{(\varepsilon_1^c - \varepsilon_0^c) + \varepsilon^d - \varepsilon_0^p\right\}\right| \quad (8)$$

$$\sigma_1^{eq} \equiv \left|\sigma_1^{in} - \sigma_1^{out}\right| = 2\left|\gamma_1\sigma - 3f_0\gamma^*\left\{(\varepsilon_1^c - \varepsilon_0^c) + \varepsilon^d - \varepsilon_0^p\right\}\right| \quad (9)$$

In considering the inelastic deformation of each phase under these micro stresses, inelastic deformations such as plastic and creep deformations are assumed to obey the associated flow rule in which both plastic and creep potentials are taken equal to the von Mises-type yield function. Actually, various kinds of constitutive relations can be taken into account for both deformations. In this study, the following are considered.

Plastic deformation of metal phase is assumed to be expressed by the Swift's equation.

$$\sigma_0^{eq} = a(c + \varepsilon^{p\,eq})^n \quad (10)$$

where a,c and n are constants. When the creep deformation of each phase is assumed to be controlled by grain-boundary diffusion, which is called Coble creep, the constitutive equation is expressed as follows

$$\dot{\varepsilon}^{c}_{coble}{}^{eq} = C\frac{\omega_{gb}D_{gb}\Omega}{kTd^{3}}\sigma^{eq} \qquad (11)$$

C is the geometric constant (~16), D_{gb} the grain boundary diffusivity, ω_{gb} the grain boundary width, Ω the volume of a diffusing atom and k the Boltsman's constant. Meanwhile, the inelastic strain $\varepsilon^{d\,eq}$ by mass transport along the interface between metal and ceramic phases is expressed as follows, according to the study by Mori et al. [26],

$$\dot{\varepsilon}^{d\,eq} = C^{int}\frac{\omega_{int}D_{int}\Omega}{kTd_{p}^{3}}\sigma_{1}^{eq} \qquad (12)$$

C^{int} is the material constant derived by the micromechanical concept, ω_{int} the interface width for diffusion, D_{int} the interfacial diffusivity and Ω the volume of diffusing atom. The equivalent stresses in equations (10), (11) and (12) can be given by equations (8) and (9). The von Mises-type equivalent inelastic strains $\varepsilon^{p\,eq}, \varepsilon^{c\,eq}, \varepsilon^{d\,eq}$ are given by $2|\varepsilon^{p}|$, $2|\varepsilon^{c}|$, $2|\varepsilon^{d}|$, respectively. Therefore, when considering the composites under plane-stress conditions, the constitutive equations can be derived as follows,

$$\begin{aligned}\dot{\sigma}(z,t) = &\left\{S^{e}(z) + S^{p}(z,t)\right\}^{-1} \\ &\left\{\dot{\varepsilon}(z,t) - \alpha(z)\dot{\theta}(z,t) - \varepsilon^{p(cd)}(z,t) - \varepsilon^{c-d}(z,t)\right\}\end{aligned} \qquad (13)$$

$\dot{\sigma}(z,t)$ is the plane stress rate, $S^{e}(z)$ the overall plane-stress elastic compliance, $S^{p}(z,t)$ the overall plane-stress plastic compliance, $\alpha(z)$ the overall in-plane thermal expansion coefficient, $\dot{\varepsilon}^{p(cd)}(z,t)$ the overall plastic strain rate due to the difference between creep abilities of each phase and interfacial diffusion, and $\dot{\varepsilon}^{c-d}(z,t)$ the over all creep strain rate. The expressions for these are given in the work[26] by Tsukamoto.

4.1.3 Modified classical lamination theory

For the macro-mechanical analysis, modified classical lamination theory, which can take into account the time-dependent inelastic deformation for each laminate, is applied. Consider the FGM plate consisting of very thin layers with thickness dz located at position z in the coordinates as shown in Figure 4-1. Let

$\dot{\sigma}(z,t)$ be the in-plane macro-stress rate, which corresponds to that shown in equation (13) reduced by the micromechanical approach. In the lamination theory considered here, the following in-plane stress rate states are assumed.

$$\dot{\sigma}(z,t) \equiv \dot{\sigma}_x(z,t) = \dot{\sigma}_y(z,t) \tag{14}$$

All other macro-stress rate components are zero. The corresponding in-plane strain rates are

$$\dot{\varepsilon}(z,t) \equiv \dot{\varepsilon}_x(z,t) = \dot{\varepsilon}_y(z,t) \tag{15}$$

Out-of-plane strain rate component is not zero. The in-plane strain rate component $\dot{\varepsilon}(z,t)$ is given using the mid-plane strain rate $\dot{\varepsilon}^0(t)$ and the curvature rate $\dot{\kappa}(t)$ according to the strain compatibility, as follows

$$\dot{\varepsilon}(z,t) = \dot{\varepsilon}^0(t) + z\dot{\kappa}(t) \tag{16}$$

In-plane force rate $\dot{N}$ and bending moment rate $\dot{M}$ (per unit edge length of the FGM plate) are related to macro-stress rate as follows

$$\dot{N}(t) = \int_{-h}^{h} \dot{\sigma}(z,t)dz \tag{17}$$

$$\dot{M}(t) = \int_{-h}^{h} \dot{\sigma}(z,t)zdz \tag{18}$$

Here, the thickness of FGM plate is 2h. Using equations (13) to (18), the following expression for constitutive relation of the FGM can be derived.

$$\begin{bmatrix} \dot{\varepsilon}^0(t) \\ \dot{\kappa}(t) \end{bmatrix} = \begin{bmatrix} A_{11} & A_{12} \\ A_{21} & A_{22} \end{bmatrix}^{-1} \left\{ \begin{bmatrix} \dot{N}(t) \\ \dot{M}(t) \end{bmatrix} + \begin{bmatrix} \dot{B}_1(t) \\ \dot{B}_2(t) \end{bmatrix} \right\} \tag{19}$$

with

$$\begin{bmatrix} A_{11} & A_{12} \\ A_{21} & A_{22} \end{bmatrix} = \int_{-h}^{h} \begin{bmatrix} 1 & z \\ z & z^2 \end{bmatrix} \left\{ S^e(z) + S^p(z,t) \right\}^{-1} dz \tag{20}$$

$$\begin{bmatrix} \dot{B}_1(t) \\ \dot{B}_2(t) \end{bmatrix} = \int_{-h}^{h} \begin{bmatrix} 1 \\ z \end{bmatrix} \left\{ S^e(z) + S^p(z,t) \right\}^{-1} \left\{ \alpha(z)\dot{\theta}(z,t) + \varepsilon^{p(cd)}(z,t) + \varepsilon^{c-d}(z,t) \right\} dz \tag{21}$$

A_{11}, A_{12} and A_{22} are dependent on the elastic and plastic constants. A_{11} is the in-plane stiffness, A_{22} is the bending stiffness and $A_{12} = A_{21}$ is the coupling stiffness. $\dot{B}_1(t)$ and $\dot{B}_2(t)$ are the in-plane force rate and bending-moment rate, respectively, due to internal stress induced by differential thermal expansion, plastic and creep deformation, and interfacial mass-transport.

3.2 CASE STUDY FOR Ni-ZrO_2 SYSTEM

4.2.1 Compositional gradation patterns and boundary conditions

In this study, we consider the thermal barrier coatings with a FGM structure characterized by the step-wised gradation of volume fraction as shown in Fig.2.

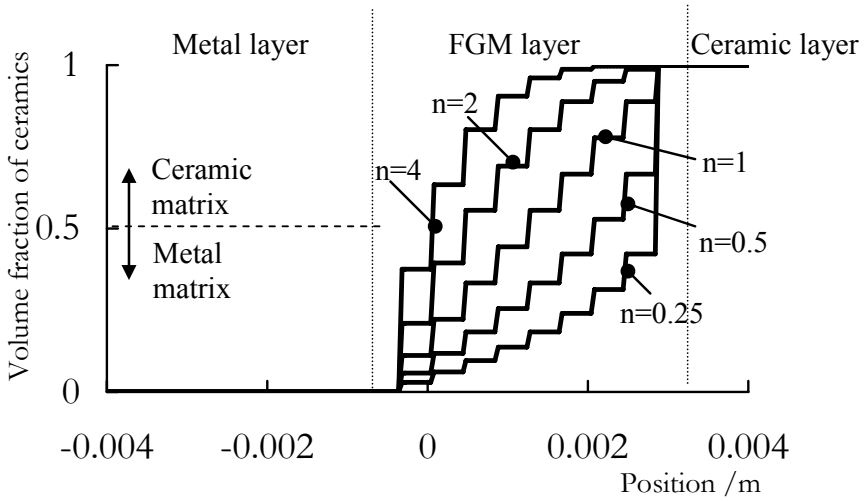

Figure 2 Compositional gradation pattern for FGM thermal barrier plates

For a parametric description of compositional gradation for an FGM layer, we define the following expressions.

$$f_m(i) = 1 - f_c(i) = \left(\frac{i-1}{P-1}\right)^n \qquad (23)$$

where, $f_m(i)$ and $f_c(i)$ are the volume fractions of metal and ceramic phases in the i-th sub-layer, respectively. P is the total number of sub-layers in a FGM layer, which have the same thickness for each and the exponent n is the parameter characterizing gradient compositional patterns. An example of representation of the patterns in an FGM thermal barrier coating is shown in Figure2. P is set at 10.

The case of n=1 indicates a linear compositional pattern, the case of n>1 indicates a ceramic-rich pattern and the case of n<1 indicates a metal-rich pattern.

Numerical study has been carried out for a Ni-ZrO_2 system, which attracts a great deal of attention as thermal barrier coatings at super high temperatures in aerospace and automobile industries. The material properties used for the calculation are shown in Table1. The creep properties for both Ni and ZrO_2 phases are shown for Coble creep. According to the studies by Berbon and Langdon[27], such grain boundary diffusion-controlled creep is dominant over a wide range of temperatures and applied stresses in ZrO_2.

Thermo-mechanical boundary conditions are set as follows. For thermal boundary conditions, firstly the temperature in the whole FGM plate is uniform at 300K, and then the stress in the FGM plate is assumed to be zero. Next, the surface of ceramic layer is heated up instantaneously to a temperature of 2000K (or 1600K) for 20 sec, while the metal surface is kept at the constant temperature of 300K all the time. Lastly, the ceramic surface is exposed to the media at an ambient of 300K and heat transfer coefficient of 100 Wm^{-2}. Fig. 3 shows the temperature transients on the ceramic surface of the TBC with a FGM structure with an n value of 1 for maximum temperatures set at 2000 and 1600K.

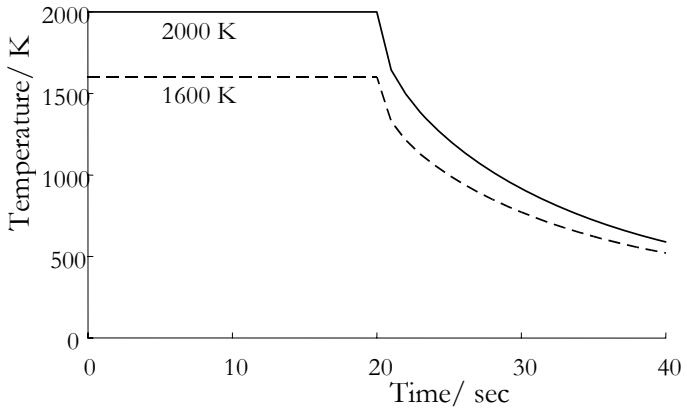

Figure3. Temperature transients on the ceramic surface for a TBC with 4mm FGM interlayer with n=1

For mechanical boundary conditions, we consider three cases. Case1 is completely stress free ($\dot{N}(t) = \dot{M}(t) = 0$), Case 2 is constraint in only out-of-plane deformation ($\dot{\varepsilon}^0(t) \neq 0$, $\dot{\kappa}(t) = 0$), and Case 3 is completely constraint in both in-plane

and out-of-plane deformations($\dot{\varepsilon}^0(t)=0$, $\dot{\kappa}(t)=0$). The FGM plate in Case1 and Case 2 correspond to high temperature-resistant panel structure like a plane body and Case 3 corresponds to a thermal barrier structure covering rigid and thick substrates.

Table 4-1. Material properties of Ni and ZrO_2 used for numerical analysis [28-29]

	Ni	ZrO_2
Young's modulus /GPa	207	200
Poisson's ratio	0.31	0.3
CTE /$10^{-6}K^{-1}$	13.3	10.0
Thermal conductivity / $Wm^{-1}K^{-1}$	89.9	3.0
Specific heat / Jkg^{-1} K^{-1}	443	3000
Density / kgm^{-3}	8890	5990
[Coble creep parameters]		
D_{gb0} (pre-exp. Term)×W_{gb} / m^3s^{-1}	3.5×10^{-11}	0.29×10^{-6}
Activation energy / $Jmol^{-1}$	1.09×10^{-29}	4.66×10^{-29}
Atomic volume / m^3	1.15×10^{5}	5.7×10^{5}
Grain size / m	10.0×10^{-6}	10.0×10^{-6}

Diameter of particle in matrix 40×10^{-6} , $D_{int}\times W_{int}$ is assumed to be the same value as $D_{gb}\times W_{gb}$ for Ni.

Flow stress parameters in Swift equation for Ni are a=600GPa, c=0.3 and n=1.

4.2.2 Effect of compositional gradation patterns

The effect of compositional gradation patterns on thermal stress states is investigated here. At first, we examine the effect of gradation pattern parameter n on the overall heat-transfer coefficient and average density of the FGMs with a certain thickness. Both parameters are very important in design of FGM TBCs from the viewpoints of thermal shielding and light weight properties. The overall heat-transfer coefficient is expressed as follows.

$$k_{FGM}=\frac{1}{2h}\left(\frac{1}{P}\sum_{i=1}^{P}\frac{1}{\lambda_i}\right)^{-1} \qquad (24)$$

Here, overall heat-transfer coefficient, k_{FGM}, is related to heat flux, q, and difference of temperatures between the ceramic and metal sides, Tc and Tm such that

$$q = k_{FGM}(T_c - T_m) \qquad (25)$$

On the other hand, the average density of FGMs is given as,

$$\rho_{FGM} = \frac{1}{P}\sum_{i=1}^{P}\left[f_m(i)\cdot\rho_{met} + f_c(i)\cdot\rho_{cer}\right] \qquad (26)$$

Figure 4 shows the overall heat-transfer coefficients and average density of an FGM layer with a fixed thickness of 4 mm as a function of gradation parameter n. As seen here, with increasing n, that is with increasing total volume fraction of ceramics in the FGMs, both overall heat-transfer coefficients and average densities get lower. As seen here, for n over 4, both the indications are almost constant, and in the following analysis, we will pay attention to the values of gradation parameter n which is 4 or below.

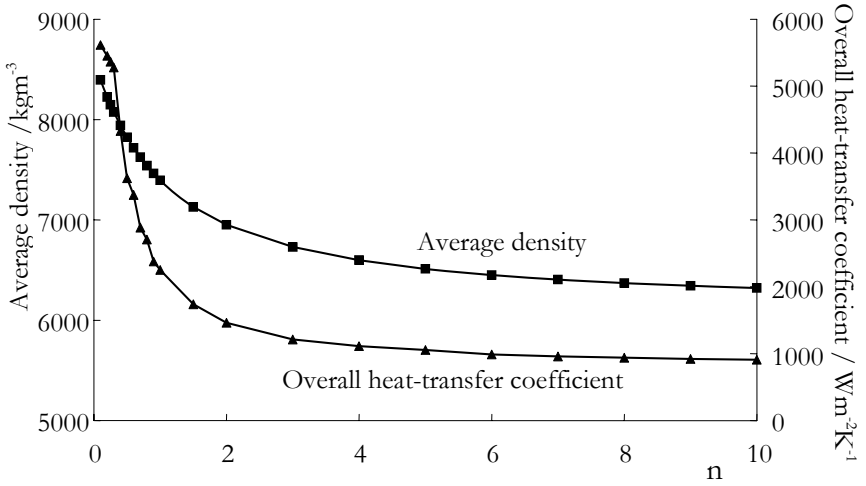

Figure 4 Overall heat-transfer coefficient and average density for an FGM interlayer as a function of n.

Fig. 5 shows the transients of maximum tensile micro-stresses generated in ceramic phases under the given thermo-mechanical boundary conditions, which can be calculated using equation (2)-(5). The maximum tensile micro-stresses considered here are focused on those which are generated in the position that volume fraction of ceramic phase is over 0.5. This is because in the case that ceramic phase is matrix in the situation of ceramic volume fraction of over 0.5, the fracture of ceramic phase can more easily lead to the fracture of the FGM plates.

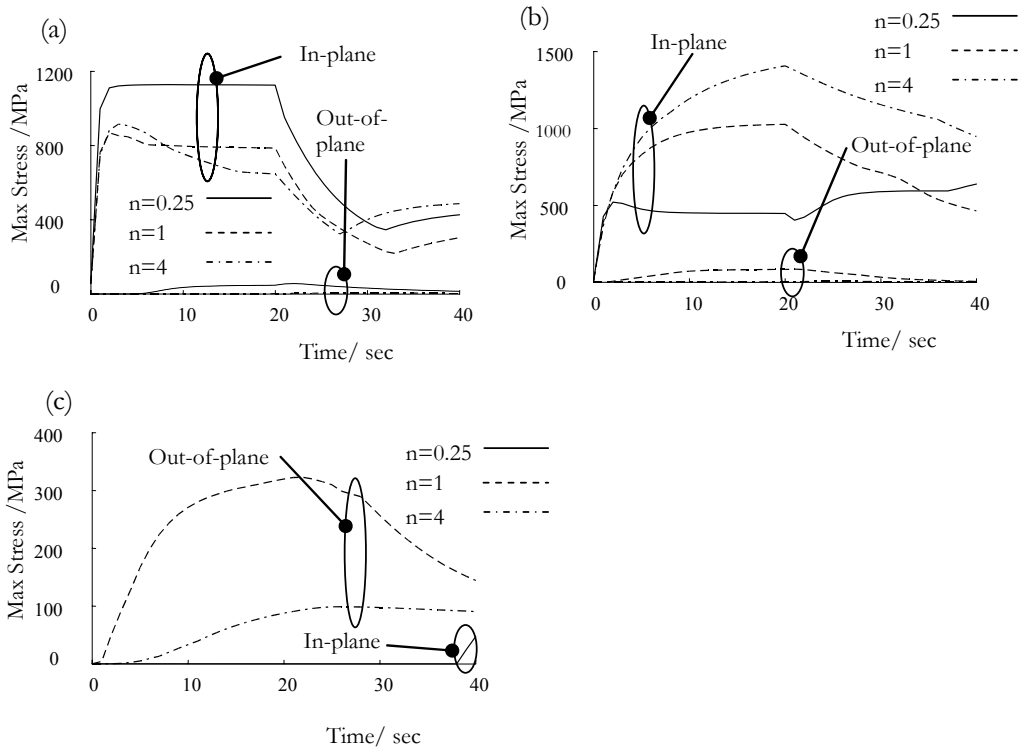

Figure 5 Maximum tensile micro-stresses transients in ceramic phases for n=0.25,1 and 4. (a) is for Case1, (b) for Case2 and (c) for Case3.

In this figure, both the in-plane and out-of-plane components in micro-stress are shown.

For Case 1 shown in (a) of Figure 5, the maximum tensile in-plane stress can be generated in the stage of heating, and the stress for n=0.25 reaches the highest value over 1.1GPa. For Case 2, the in-plane stress for n=4 is the highest. In both case 1 and 2, the out-of-plane tensile micro-stresses are very low all the time. For Case 3,

micro-stresses in ceramic phases are also relatively low, while the out-of-plane stress components are higher than the in-plane stresses.

Figure 6 shows the maximum micro-stresses in ceramic phases and the volume fraction in the position that the maximum micro-stresses are generated as a function of compositional gradation parameter n. In this figure, the results for the case that the thicknesses of FGM layers are 4mm and also 8mm, and the maximum temperatures on the ceramic surface of 2000K and 1600K are shown. For Case 1 shown in (a) of Figure 8, the maximum micro-stress for n=5 is the lowest, and the volume fraction in the position where this maximum stress is generated is also lower than those for other values of n. This means that n=0.5 is the most suitable to prevent thermal-induced fracture for Case 1. For Case2, the less values of n are, the less maximum tensile stresses are generated, but considering the volume fractions of ceramics for the maximum stresses, n=0.5 seems to be the best selection. For Case3, the volume fraction that maximum stresses are generated is relatively constant, so n=4 is the most suitable. As seen here, we can design FGM TBCs from the view points of reduction of tensile micro-stresses in ceramic phase as well as improvement in thermal shielding and light weight properties as mentioned above.

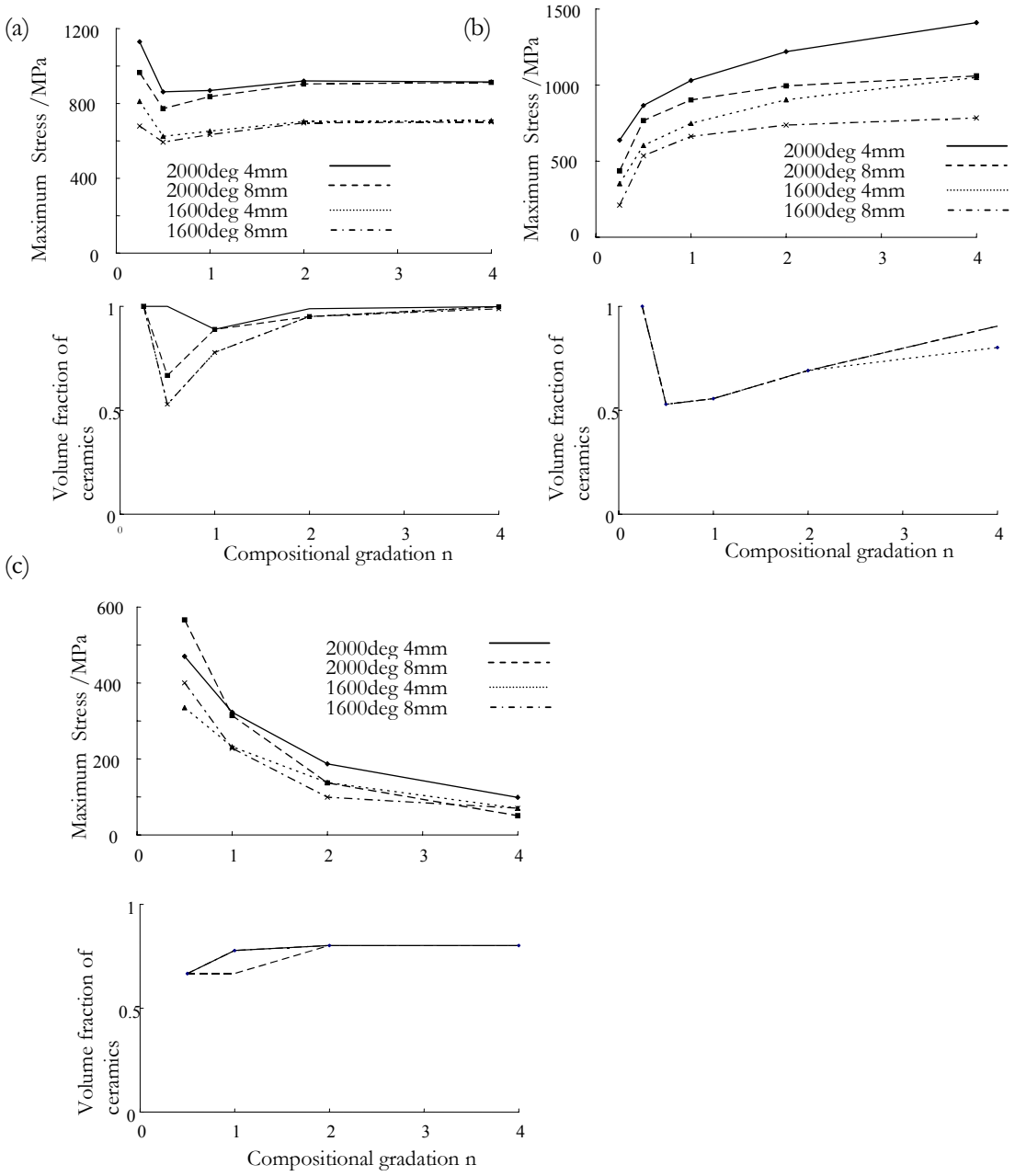

Figure 6 Maximum tensile micro-stresses in ceramic phases and volume fraction of ceramics at the position they are generated as a function of compositional gradation pattern. In-plane stresses for Case 1 (a), Case 2 (b), and out of plane stresses for Case3 (c).

4.3.3 Effect of creep of ZrO_2

In this numerical study, the creep deformation of ZrO_2 is assumed to be expressed by the Coble creep equation, so the creep rate is inverse proportional to the grain size to the power of three as seen in equation (11). The grain size has a big influence on the creep rate in this creep mechanism. In the above calculation, we set the grain size of ZrO_2 as 10μm, and the creep deformation almost does not occur in ZrO_2 phase with this grain size under the given thermo-mechanical boundary conditions. In the following, the influence of grain size of ZrO_2 on the stress states in the Ni-ZrO_2 FGM plate will be examined. Figure 7 shows the macro-stress distributions in the FGM plate with grain size of the ZrO_2 being 1μm at 3, 20 and 40sec for Case1. At 20 sec, the compressive stress generated near the ceramic surface is relaxed by the creep deformation of ZrO_2, and then, in the cooling stage, the extremely large tensile stress is generated on the ZrO_2 surface due to this creep effect, which possibly leads to the fracture of ZrO_2 surface layer. In this way, the creep of ZrO_2 can bring a serious problem to cause thermal fracture at the cooling stage, so it is very important to control this creep to prevent such a fracture. The experimental data in which fracture on the ceramic surface of FGM thermal barrier structures occurs due to the creep have been reported by some researchers [30].

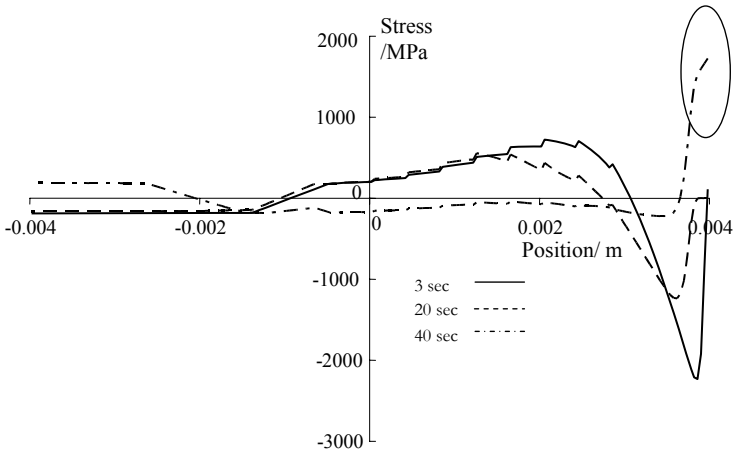

Figure 7 Macro-stress distributions in a FGM TBC with a ZrO_2 of grain size of 1μm at 3, 20 and 40sec for Case1. The FGM layer has a thickness of 4mm, and the maximum temperature of ceramic surface is 2000K.

Figure 8 shows the relation between maximum tensile stresses in the ZrO_2 surface layers and grain sizes of ZrO_2 for the FGM thermal coating with the thickness of FGM layer being 4mm, in which the temperature of the ZrO_2 surface rises to 2000K. As seen here, when the grain size is 1μm, the highest tensile stresses are generated for any gradation parameter n of 0.25 1, and 4, and any mechanical boundary conditions. This grain size of ZrO_2 should be avoided so as not to cause thermal fracture and prevent creep of ZrO_2 in practical situations.

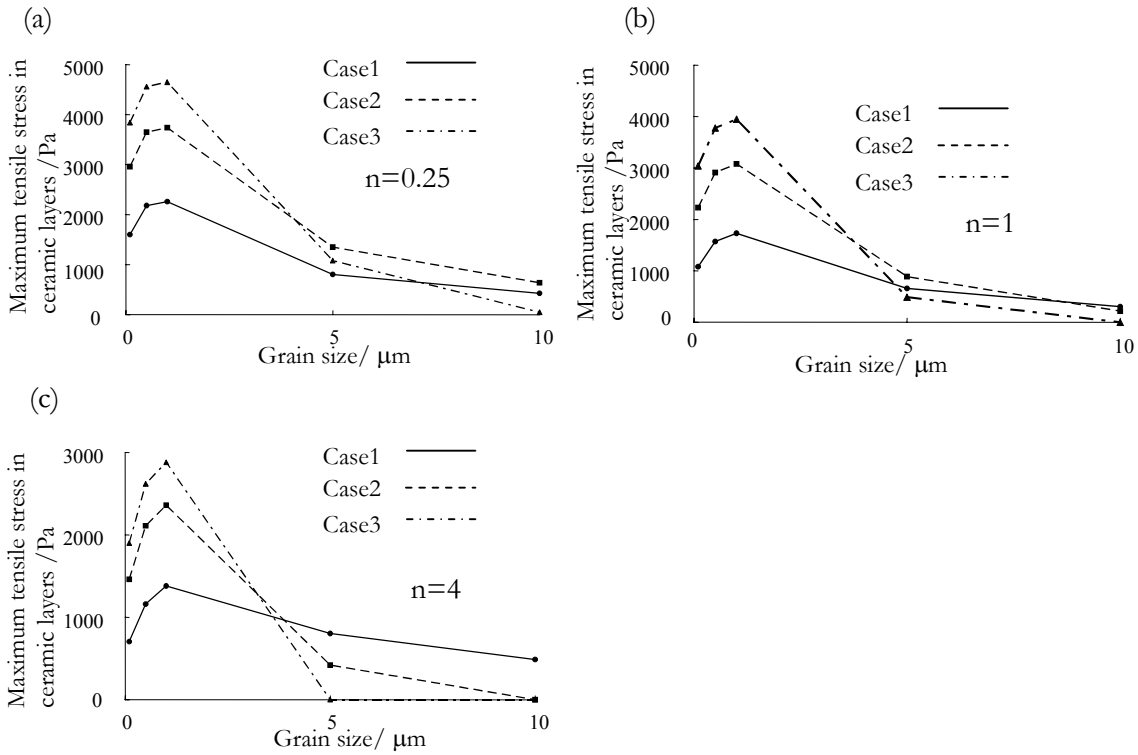

Figure 8.
Maximum tensile stresses in ceramic layers as a function of grain sizes of ZrO_2

Thermal-Structural Modelling of Hypersonic Structures

The high temperatures associated with hypersonic flights will reduce fatigue life by firstly, a reduction in material strength and fatigue resistance at elevated temperatures and secondly, the high thermal gradients will result in internal strains[7, 8]. This section of the report presents a relatively simple and quick method for predicting the aero-thermal-structure response of hypersonic structures that can be adopted / modified to implement the FGM micromechanics models. The predictive capability described here has been utilised, as part of the design strategy, in the aero-thermal-structural analyses of the DARPA HyCause dual-mode scramjet engine[7] and the USAF/DSTO HiFire 1 hypersonic vehicle for flight tests. This tool[8] was used to predict the temperature distribution as well as the structural deformation (for example, bulging, distortion of engine throat) due to the aerothermal heating loads during re-entry into the atmosphere, in order to identify critical design factors and optimise the structural design.

For the non-linear transient thermal-structural analysis, aerodynamic heating models for varying trajectory points were implemented in our finite element code. The aerodynamic and combustion models for varying spatial position and trajectory points were developed using CFD (computational fluid dynamics) data or measured from shock tunnel experiments or calculated using engineering level approximate methods (such as the Eckert Reference Enthalpy and Fay Ridell stagnation point analysis). Our FEM approach for thermal-structural-vibrational analysis of hypersonic structures has several capabilities / features, including temperature dependent constitutive models of thermally degrading materials, the heat flux can be varied with spatial position and time for changing trajectory points and combined thermal and pressure loading which can be varied for changing altitudes.

The heat fluxes from the aerodynamic heating and combustion models were interpolated onto the 3D FE thermal-structural models for each time-step in the transient thermal analysis using user defined algorithms. The thermal loading was applied as a time varying heat flux condition to model the change in environment at various altitudes in the flight trajectory. Using the calculated temperature-time history from the transient heat analysis, a non-linear transient dynamics analysis was conducted to predict the thermal stresses and deformation in the vehicle during the thermal transient.

To accurately predict the stresses and strains induced by the thermal transient simulating the flight trajectory, temperature dependent non-linear constitutive models were developed and implemented in the transient dynamics solver of the finite element program. Experimental results from an induction heating method for measuring high temperature material properties[31], such as thermal expansion coefficient (CTE), Young's modulus of elasticity and stress-strain behaviour as functions of temperature, were used to develop high temperature constitutive models, in a form that can be implemented in finite element analysis (FEA). At a given temperature, the constitutive equation has the form

$$\sigma(T) = E'(T)\varepsilon^m \qquad (27)$$

where σ is the stress, ε is the strain (calculated from the temperature dependent CTE values), E' is the Young's modulus of elasticity, m is the strain exponent respectively and T is the temperature. In phase 2 of this project, constitutive models of FGM's will be developed using the micromechanics approaches described in Section 4 of this report for implementation in the thermal-structural FE code.

Some results from our aero-thermal-structural and thermal-structural-vibrational analyses are presented below, using a Mach 10 generic HyShot scramjet engine to illustrate the modelling strategy. A 3-D FE model of the intake and combustor is illustrated in Figure 5-1. The scramjet has a tungsten leading edge, an Aluminum alloy (6061-T6) intake comprising three ramps with different wedge angles and a Copper alloy combustor. The FE analysis was carried out for a for a transient thermal loading that is typical of aerodynamic heating conditions for a Mach 10 flight during re-entry into the atmosphere. The descent trajectory from 60 to 26 km was considered here as this is the region that is most critical for structural design.

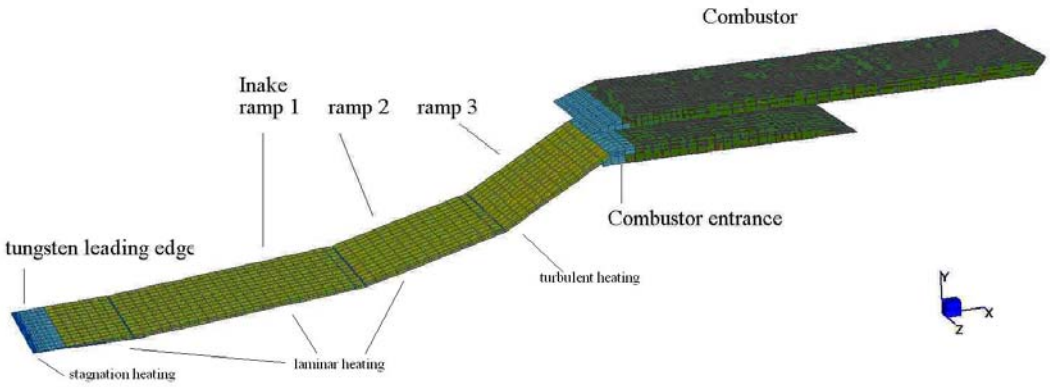

Figure 5-1: 3-D FE model of the combustor and intake of a M10 generic HyShot engine

In this example, the vehicle geometry is relatively simple and the aerodynamic heating loads were predicted using engineering level approximate methods (described in detail in reference 8) to calculate aerodynamic heating fluxes as functions of spatial position and time for varying trajectory points. The results of the aeroheating fluxes at various positions along the intake ramps as a function of altitude, presented in Figure 5-2, were utilised in the FE transient thermal analysis to capture the fluid-thermal interaction. The Eckert Reference Enthalpy and Fay Riddell stagnation point approximate methods were sufficiently accurate (within ±10-20%) for simple geometries. However, for more complex vehicle geometries we have adapted our aero-thermal-structural analysis method to incorporate aerodynamic heating fluxes, which varied with spatial position and altitude, from CFD analysis into the FE models[7]. Similarly, combustion heat fluxes from shock tunnel experiments or theoretical calculations have been implemented in the coupled thermal-structural analysis.

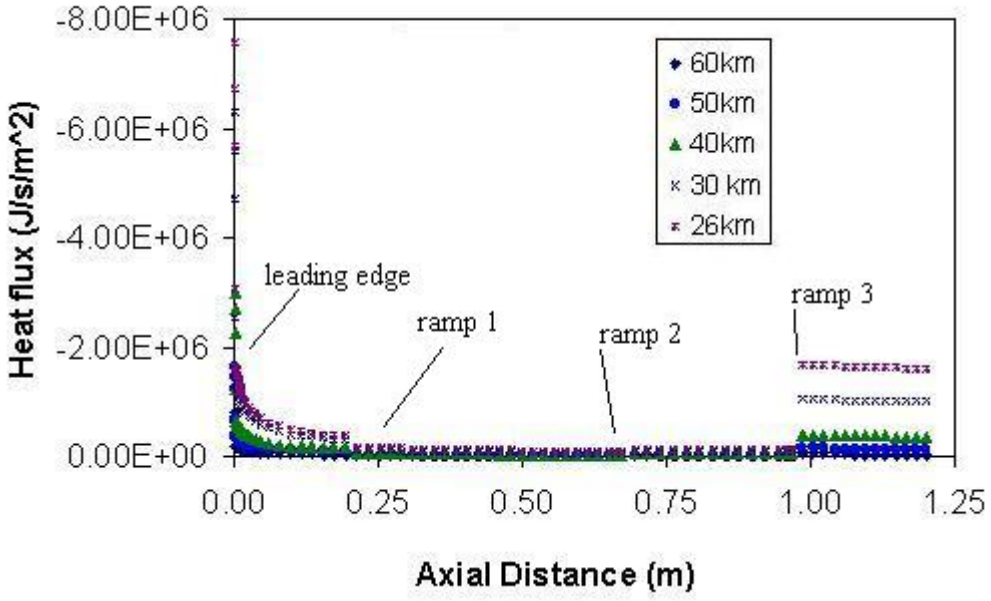

Figure 5-2: Heat flux as a function of axial distance and altitude

Aero-thermal-structural analysis

For the sake of simplicity, only the thermal-structural results of the intake ramps, where aerodynamic heating is most significant, are reported here. The temperature contours in the intake ramps, with a plate thickness of 15 mm and nose radius of 2 mm, at the start and end of the thermal transient are shown in Figures 5-3(a-b). Plots of temperature as a function of time (altitude) for the leading edge and the third ramp are shown in Figure 3-4. As expected, the highest temperature (ca. 2008K) is at the leading edge, due to stagnation point heating. The temperatures increase exponentially with decreasing altitude. The difference between laminar and turbulent convective heat transfer is quite substantial at the end of the thermal transient – the temperature in the third ramp is 512K, approximately 190K higher than in the second ramp. Radiative heat transfer from the body surface to ambient temperature was found to have little effect in the relatively short time-scale of this analysis.

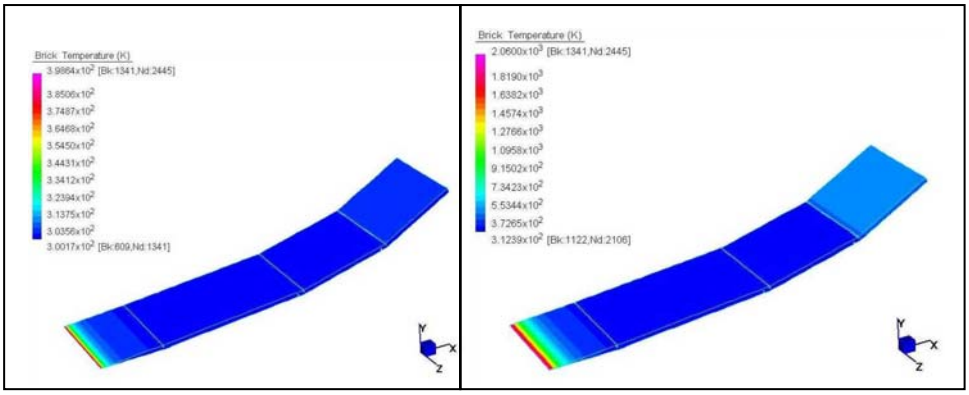

(a) (b)

Figure 3-3: Temperature distribution in intake ramps at the (a) start and (b) end of thermal transient

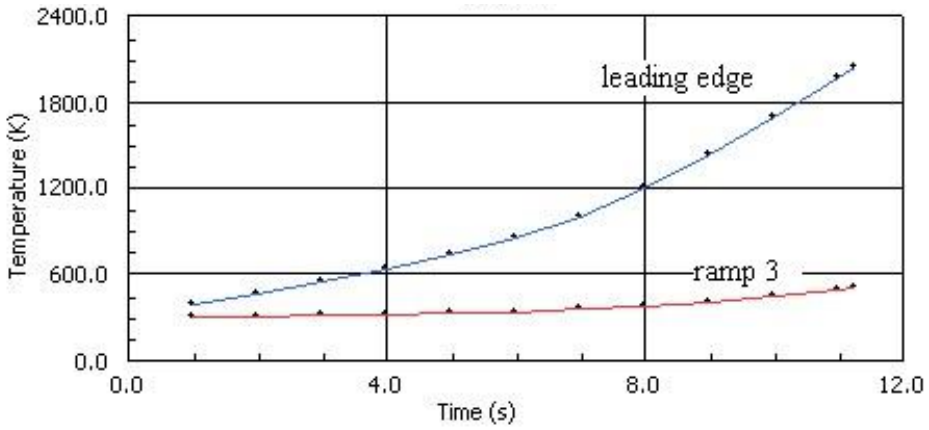

Figure 3-4: Temperature as a function of time for leading edge and third intake ramp

To assess the likelihood of engine geometry distortion, the resulting thermal loads from the thermal analysis were used in the transient dynamic analysis to predict the deformation and stress-strain state of the structure during the thermal transient. Temperature-dependent material properties (Young's modulus, thermal expansion coefficient, thermal conductivity, and specific heat capacity) were used where available. The deformed shape of the displacement contours in the intake at 30 km altitude (time ≈ 10 s) is shown in Figure 3-5. It shows bulging in the third ramp and

to a lesser extent in the second ramp, in a manner consistent with a high temperature gradient between the upper and lower surfaces of the plate and constraint by the sidewalls. The maximum vertical displacement (DY) in the third ramp at 30 km altitude (time ≈ 10 s) is around 0.5 mm (10-mm plate model). The displacement contours also show the leading edge moving forward and the third ramp slipping towards the 3-mm gap, designed for stress relief, between the second and third ramps. The maximum axial displacement (DX) at 30 km altitude is 0.8 mm, in the leading edge (10-mm plate model).

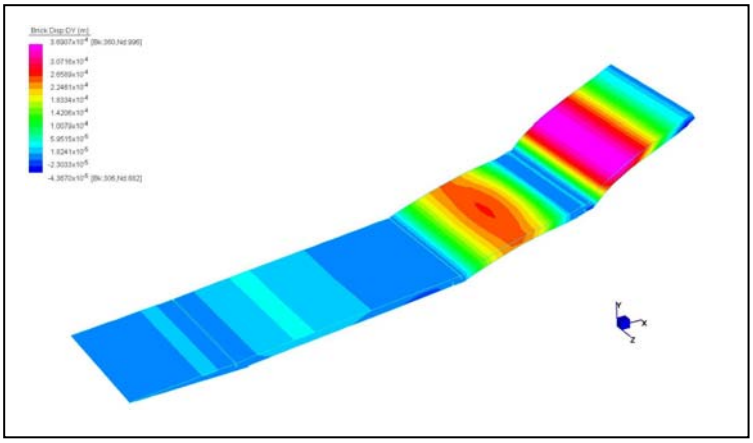

Figure 3-5: Displacement contours from transient thermal analysis at 10 s (30 km altitude) for FE model. Displacement scale = 1%

Von Mises stress and strain contours in the intake ramps at 30 km altitude (time ≈ 10 s) are shown in Figures 3-6. The transient thermal loads induce stresses and strains in the scramjet mainly by the large temperature gradients and, to a lesser extent, the difference in thermal expansion coefficients between the leading edge material and the intake ramps material. The structural analysis predicts that the highest stresses are in the tungsten leading edge, as expected.

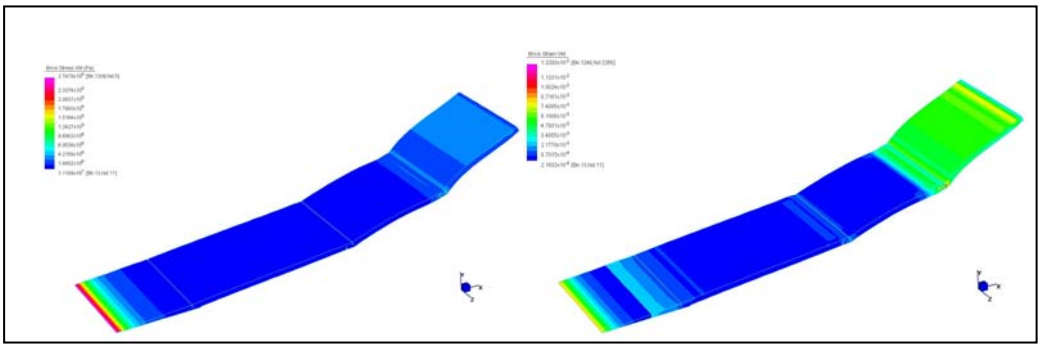

(a) (b)

Figure 3-6: (a) von Mises stress and (b) strain contours in intake ramps at 10s (30 km altitude) for FE model.

Structural Vibration Modes Analysis

A structural-vibrational analysis is conducted to understand the effects of the aero-acoustic loads (for example, long thin structures are subjected to elastic bending in low frequency vibration modes and the stiffness characteristics of these modes change due to surface heating). The natural vibration modes of the scramjet engine may be excited by flow disturbances (aerodynamic and combustion). The modal shapes and natural frequencies of the model of the intake (10-mm plate) and combustor together, at a uniform temperature of 300 K, are shown in Figure 3-7. The lowest natural frequency of this model is at 118 Hz, attributed to bending of the upper plate of the combustor. The mode 3 deformation is at 306 Hz and corresponds to bending of the first intake ramp.

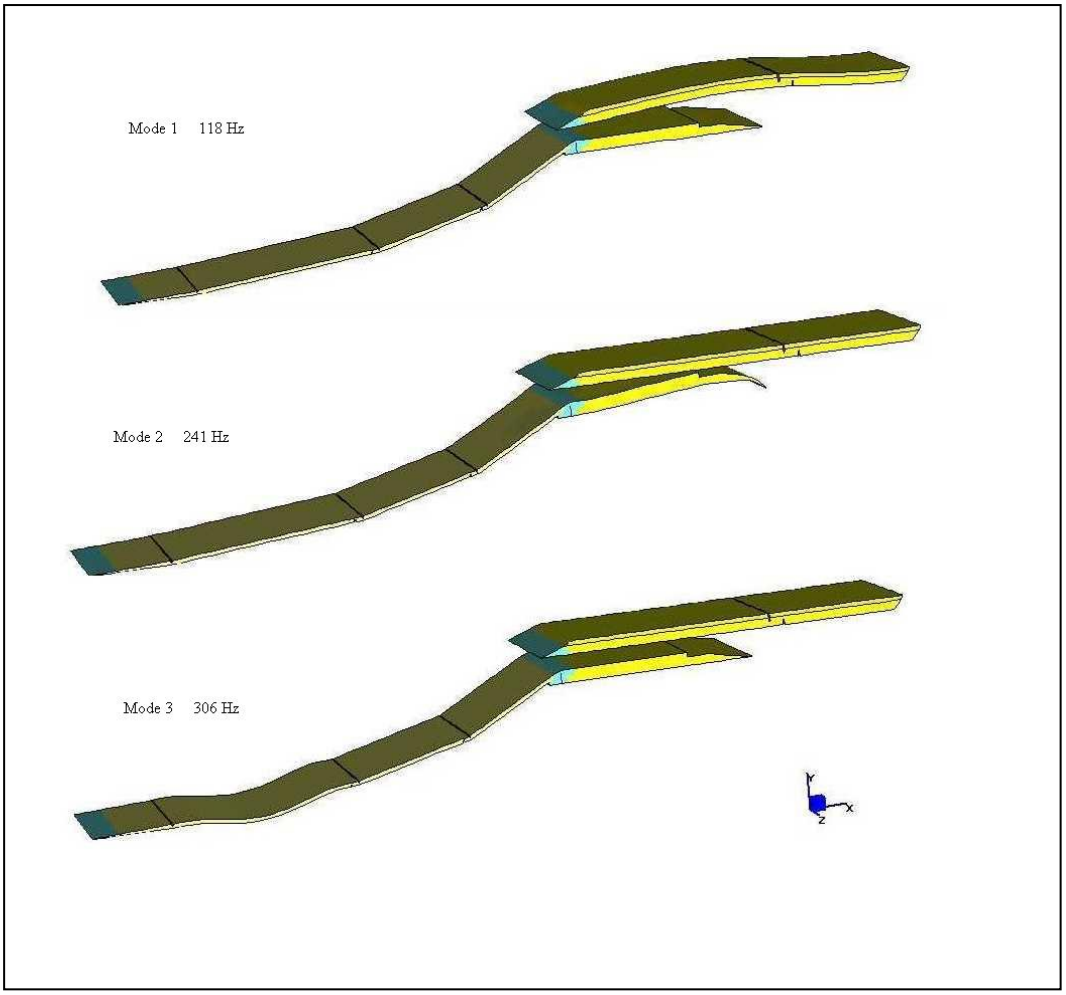

Figure 3-7: Vibration modes and frequencies of combustor and intake at a uniform temperature of 300K. Displacement scale = 1.5%

A vibration analysis was performed following the thermo-structural analysis to determine the changes in natural frequencies of the structural vibration modes that occur at the various temperatures associated with the descent trajectory from 60 to 26 km. The vibration characteristics of the intake ramps (10-mm plate) at 30 km altitude are compared with those at a uniform ambient temperature (300 K) in Figure 3-8. The mode 1 natural frequency of this model (corresponding to bending of the first intake ramp) is 306 Hz at 300 K and shifted to 302 Hz at 30 km altitude. These results indicate that the lowest natural frequency of this engine (see Figure 9) is high - the engine behaves as a rigid body for the given trajectory and. However, for operation at low altitudes over a longer period of time (for example, during a pull-up manoeuver and cruising), aerothermoelastic effects could become more significant. In addition to

using this thermo-structural vibration analysis capability as a structural design tool, it could also help in the design of control systems to compensate for aerothermoelasticity.

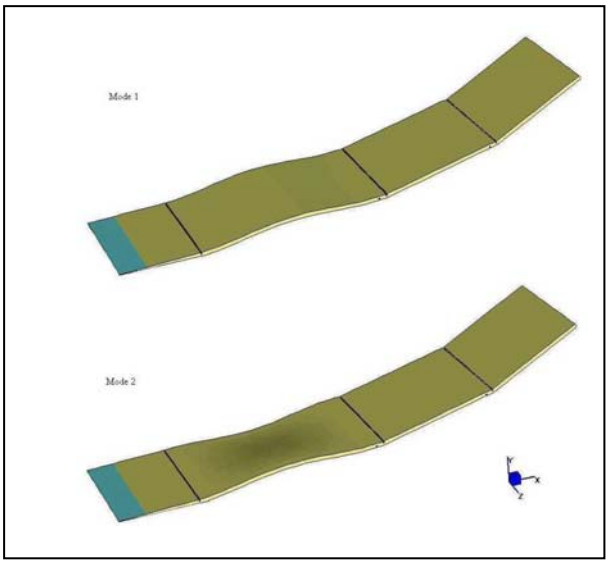

	Frequency (Hz)	
	300K	30 km
Mode 1	306	302
Mode 2	505	500

Figure 3-8: Vibration frequencies of intake at a uniform temperature of 300K and 30 km altitude. Displacement scale = 1.5%

6. Summary and Future Plans

A feasibility study of a relatively simple and economical method for producing functionally graded thermal barrier coatings using the Wet Powder (Slurry) and Sintering method showed promising results. This method is relatively undeveloped and under utilised compared to more expensive techniques such as chemical vapour deposition, physical vapour deposition, plasma spraying and powder metallurgy. It utilises a pressurised spray gun to spray a slurry mixture of the powdered coating material suspended in a liquid solution directly onto a substrate surface followed by sintering using an oxyacetylene torch.

The effects of slurry composition, type of ceramic powder, compatibility with substrates, spraying and sintering conditions were studied. Several TBC specimens have been fabricated under various conditions to develop a procedure which produce good quality coatings (of up to 3 layers) with little or no spallation. The optimum time, heat flux and applied pressure level for sintering were deduced. TBCs produced from a 40-45% ceramic, 4% binder and 0.4% dispersant composition and sintered for 30 minutes with an applied pressure of 30 MPa produced good quality coatings with a uniform and very smooth surface. Scanning electron micrographs of the fabricated TBC coatings showed good contact between the grain boundaries of the ceramic powder.

In phase 2 of this project, the Wet Powder and Sintering method will be further developed. Improvements to this method include automating the sintering procedure and optimising the fabrication conditions. A much more extensive micromechanical testing program will be conducted to obtain a more qualitative measure of the quality of the FGM thermal barrier coatings and to develop high temperature constitutive models for input into the FE modelling. Additionally, the TBCs will be applied to realistic hypersonic structures such as a cylindrical combustor and tested under realistic combustion conditions.

The mean-field micromechanical approach was applied to design ceramic-metal FGM thermal coatings. This analysis took into consideration the microscopic inelastic deformation in each constituent phase such as plastic and creep, as well as the diffusional mass flow at the interface between ceramic and metal phases. Through the investigation of a case study for Ni-ZrO_2 FGM TBCs, the fundamental strategy to

seek for optimal ceramic-metal FGMs was proposed. From the viewpoints of overall heat-transfer coefficient and average density of the FGM, it is better that gradation parameter n is larger, which means average volume fraction of ceramic phase is larger. Therefore, based on this strategy, it is conducted to set the gradation parameter n larger within the range that thermal fracture does not occur. For various mechanical boundary conditions, the most suitable compositional parameters were decided. Creep of ceramics near the ceramic surface has a big influence on the thermal stress states in FGMs, which can cause extremely large tensile stress during the cooling process. In order to prevent thermal stress-induced fracture due to creep of ceramics, creep of ZrO_2, which can be a cause of thermal fracture, should be avoided. Both promoting and preventing creep of ZrO_2 should be selected in practical situations. Extensive experimental work is needed to validate these numerical results obtained here and this is planned for phase 2 of this study.

An analytical method, developed in an earlier study by one of the authors, to predict the thermal-structural-vibrational response of hypersonic vehicles was presented. This aero-thermal-structural analysis capability provided a unique and relatively simple structural design tool for high-speed aerospace vehicles to identify critical design issues, optimising wall thickness and material selection, as well as providing the structural dynamics data to assist in the modelling and control of aerothermoelasticity. This tool will be used in phase 2 of this project to assist the design of FGM thermal barrier coatings at the material and global levels. At the material level, the micromechanics models described in Section 4 of this report will be implemented in the FE models of the FGM TBCs to determine the number of layers required to protect the metal structure (substrate), for example the leading edge and combustor), from the aerodynamic and combustion heating loads seen in hypersonic flights.

References

1. K. Wakashima and H. Tsukamoto, *Proc. of the 1st Int. Symp. on Functionally Gradient Materials*, FGM Forum, (1990), pp.19-26
2. K. Wakashima, H. Tsukamoto and T. Ishizuka; Proc. *of the 13th Risφ Int. Symp. on Metall. Mater. Sci*., Risφ National Laboratory, (1992), pp.503-510.
3. H. Tsukamoto, A. Kotousov, S.Y. Ho, J. Codrington, Proceedings of the Structural Integrity and Failure Symposium, (2006) pp. 25
4. K. Wakashima and H. Tsukamoto: *Proc. of the 1st Int. Symp. on Functionally Gradient Materials*, FGM Forum, (1990), pp.19-26.
5. K. Wakashima, H. Tsukamoto and T. Ishizuka; Proc. *of the 13th Risφ Int. Symp. on Metall. Mater. Sci*., Risφ National Laboratory, (1992), pp.503-510.
6. H. Tsukamoto and A. Kotousov, *Key Engineering Materials,* Vols. 340-341 (2007) pp. 95-100
7. S.Y. Ho and A. Paull, *Aerospace Science and Technology*, 10 (2006) pp. 420-426
8. S.Y. Ho, Proceedings of the *14th AIAA.AHI Space Planes and Hypersonic Systems and Technologies Conference,* AIAA-2006-8070, (2006).
9. S. Harding, Final Year Project Preliminary Report, University of Adelaide (2007)
10. DC Callister, *Funadmentals of Materials Science and Engineering*, 5th edn, 2003, Wiley, NY.
11. M Fevre, A Finel & R Caudron , 'Local order and thermal conductivity in yttriastabilized zirconia', *Laboratoire d'Etude des Microstructures*, Onera, Chatillion, France, 2004.
12. A Ruder, HP Buchkremer, H Jansen, W Mallener & D Stover, 'Wet powder spraying – A process for the production of coatings', *Surface and Coatings Technology Journal*, 1992, vol. 53, pp. 7174.
13. E.P Degarmo, JT Black & RA Kohser, *Materials and Processes in Manufacturing*, 9th edn, 2003, Wiley International, USA
14. P Roy, G Bertrand & C Coddet, 'Spray drying and sintering of zirconia based hollow powders', *Powder Technology Journal*, 2005, vol. 157, pp. 20-26.
15 Mills, AF 1999, *Heat Transfer*, 2nd edn, PrenticeHall, Sydney
16. A. E. Giannakopoulos, S. Suresh, M. Finot and M. Olsson: *Acta Metallurgica et Materialia*, 1995, vol. 43 (4), pp. 1335-1354.

17. M. -J. Pindera and P. Dunn: *Composites Part B: Engineering*, 1997, vol. 28(1-2), pp. 109-119.
18. M. Grujicic and Y. Zhang: *Materials Science and Engineering A*, 1998, vol. 251 (1-2), pp. 64-76.
19. J. Aboudi, M. -J. Pindera and S. M. Arnold: *Composites Part B: Engineering*, 1999, vol. 30 (8), pp. 777-832.
20. J. D. Eshelby: *Proc. R. Soc. London*, 1957, A241, pp. 376-396.
21. J. D. Eshelby:*Proc. R. Soc. London,* 1959, A252, pp. 561-569.
22. J. D. Eshelby: *Prog. Solid Mech.*, 1961, vol. 2, pp. 89-140.
23. M. Taya, J. K. Lee and T. Mori: *Acta Materialia*, 1997, vol. 45 (6), pp. 2349-2356.
24. K. Tohgo, A. Masunari and M. Yoshida: *Composites Part A*, 2005, in Press.
25. H. Tsukamoto: *Composites Part B*, 2003, vol. 34 (6), pp. 561-568.
26. T. Mori, M. Okabe and T. Mura, *Acta Metall.*, 1979, vol. 28, pp.319-325.
27. M. Z. Berbon and T. G. Langdon, *Acta Mater.*, 1998, vol. 46, pp.2485-2495.
28. N. G. Pace, G. A. Saunders, Z. Stimengen, and J. S. Thorp: *J. Mater. Sci.*, 1969, vol. 4, pp. 1106-l 110.
29. H. J. Frost and M. F. Ashby: *Deformation Mechanism Maps*, Pergamon Press, Oxford, 1982.
30. A. Kawasaki and R. Watanabe: *Engineering Fracture Mechanics*, 2002, vol. 69 (14-16), pp.1713-1728.
31. J. Codrington, P. Nguyen, S.Y. Ho and A. Kotousov, *Applied Thermal Engineering Journal,* submitted May 2007.